Common patterns of spatial selectivity in early visual cortex and face-selective brain regions

Anisa Y. Morsi[1], Hugo T. Chow-Wing-Bom[1,2], D. Samuel Schwarzkopf[3], Valérie Goffaux[4,5], Tessa M. Dekker[1,2], & John A. Greenwood[1]

[1]Experimental Psychology, University College London, UK

[2]Institute of Ophthalmology, University College London, UK

[3]School of Optometry & Vision Science, University of Auckland, New Zealand

[4]Psychological Sciences Research Institute, UCLouvain, Belgium

[5]Institute of Neuroscience, UCLouvain, Belgium

Short title:	Common selectivity in early & face-selective cortex
Corresponding author:	John Greenwood
Email:	john.greenwood@ucl.ac.uk
Address:	UCL Experimental Psychology, 26 Bedford Way, London WC1H 0AP

Abstract

Face recognition relies on dedicated brain regions with unique selectivity, including sensitivity to face inversion. The spatial selectivity of these regions has similarly been argued to be either unique or wholly invariant to face location, contrary to accounts of common 'visuospatial coding' whereby high-level category-selective areas inherit spatial properties from earlier regions. Because early cortical regions (V1-V3) show characteristic retinotopic variations, with greater cortical sampling along the horizontal vs. vertical meridian and in the lower vs. upper field, we examined whether face-selective regions (OFA, pFus, mFus) share these spatial anisotropies, and whether these properties could drive observed variations in face perception. Large-field upright and inverted face stimuli (±21° eccentricity) were used for retinotopic mapping and population receptive field (pRF) analyses. While pRFs were considerably larger in face-selective regions than in V1-V3, their size did not vary consistently in the direction of behavioural anisotropies. However, both early and face-selective areas showed higher pRF numbers and a concomitant increase in visual field coverage along the horizontal vs. vertical meridian and in the lower vs. upper field. Variations in face-recognition abilities around the visual field could therefore reflect these sampling differences. We also show that pRF numbers in mFus were greater for upright than inverted faces, which could in part support the perceptual advantage for upright faces. These shared variations in visual field sampling between face-selective and early visual cortex support a hierarchical model whereby the spatial selectivity of higher-level areas builds on that of earlier regions, even for specialised face processing.

Keywords

Retinotopic organisation, visual cortex, face perception, spatial vision, specialisation.

Introduction

Face recognition is crucial to everyday life, though its complexity presents challenges for the visual system (Bruce and Young, 1986). This combination has been argued to drive the 'special' nature of face processing, with a network of specialised brain regions (Kanwisher et al., 1997; Haxby et al., 2000; Grill-Spector et al., 2017) that show disproportionate disruption to face inversion (Kanwisher et al., 1998) and either complete invariance to the position of faces in the visual field (Tanaka, 1996) or distinct patterns of spatial selectivity compared with early visual cortex (Avidan and Behrmann, 2021; Poltoratski et al., 2021). This apparent uniqueness contrasts with proposals for 'canonical computations' in the brain (Miller, 2016) and growing evidence for common 'visuospatial coding', where high-level category-selective regions retain aspects of the retinotopic organisation from lower-level areas (Groen et al., 2022). We tested this discrepancy between category-selective and early cortical regions using population receptive field (pRF) mapping (Dumoulin and Wandell, 2008), examining whether face-selective regions retain the characteristic retinotopic anisotropies of early visual cortex, and whether this selectivity could explain variations in face perception around the visual field.

A ubiquitous feature of our visual abilities is their variation with polar angle around the visual field, as seen with acuity, contrast sensitivity, and crowding, where performance is best along the horizontal vs. vertical meridian (horizontal-vertical anisotropy) and in the lower vs. upper visual field (upper-lower anisotropy; Carrasco et al., 2001; Westheimer, 2003; Abrams et al., 2012; Greenwood et al., 2017; Himmelberg et al., 2020; Barbot et al., 2021). Variations in the retinotopic properties of early visual cortex have been argued to drive these performance anisotropies. In areas V1-V3, smaller pRFs have been found along the horizontal (vs. vertical) meridian (Silson et al., 2018; Silva et al., 2018), though an upper-lower anisotropy in pRF size is less consistent (Silva et al., 2018; Himmelberg et al., 2023b). More consistently, V1 shows greater surface area along both the horizontal vs. the vertical meridian and in the lower vs. upper field (Amano et al., 2009; Himmelberg et al., 2023b). This differential sampling of the visual field within early visual cortex could therefore drive the characteristic variations of low-level vision.

Recent behavioural research shows similar anisotropies for face perception, with better recognition along the horizontal vs. vertical meridian and in the lower vs. upper field (Roux-Sibilon et al., 2023; Morsi et al., 2024). Whether these anisotropies reflect variations in face-selective brain areas is unclear. Despite initial findings that face-selective areas are invariant to visual-field location (Tanaka, 1996), recent analyses reveal clear retinotopic organisation – pRFs increase in size with distance from fixation and over-represent the fovea (Kay et al., 2015; Finzi et al., 2021; Silson et al., 2022), as in earlier areas (Amano et al., 2009). Oddly however, pRFs were larger for upright vs. inverted faces (Witthoft et al., 2016; Poltoratski et al., 2021). Because recognition is best for upright faces (Yin, 1969; Rossion and Gauthier, 2002), this suggests that larger pRFs and associated increases in visual field enhance face recognition (Avidan and Behrmann, 2021; Poltoratski et al., 2021). This relationship diverges from early visual cortex, where smaller receptive fields are associated with better acuity (Duncan and Boynton, 2003; Silva et al., 2021). The 'uniqueness' of higher-level face-selective regions may therefore extend to their spatial selectivity.

These findings highlight a puzzling dissociation between low- and high-level vision. To address this, we used wide-field retinotopic mapping with face stimuli to compare the visual-field variations in three retinotopic properties (pRF size, pRF number/quantity, and visual field coverage) in early visual areas V1-V3 and core regions of the face-processing network: the occipital face area (OFA), and the posterior (pFus) and medial (mFus) fusiform gyrus which comprise the Fusiform Face Area (FFA). To assess whether these spatial properties can further drive the selectivity for face inversion in these regions, we also compared these retinotopic properties with upright and inverted face stimuli.

Methods

Design. To compare visual field variations in pRF size, pRF number, and visual field coverage, we undertook retinotopic mapping procedures with bars of either upright or inverted face stimuli. If face-selective regions (OFA, pFus, and mFus) share their *spatial selectivity* with earlier regions V1-V3 (Groen et al., 2022), these properties should vary

similarly, with e.g. smaller pRFs, higher pRF numbers, and greater coverage along the horizontal vs. vertical meridian and in the lower vs. upper field. Alternatively, if the spatial selectivity of face-selective regions reflects specialised mechanisms, whereby large receptive fields benefit face perception (Witthoft et al., 2016; Avidan and Behrmann, 2021; Poltoratski et al., 2021), we might instead observe either wholly unique variations or a reversal of the spatial selectivity in face-selective regions. To further test the link between this spatial selectivity and the stimulus selectivity of face-selective regions (i.e. the face inversion effect), we also sought to replicate prior findings that pRF sizes are larger and visual field coverage greater for upright vs. inverted faces (Poltoratski et al., 2021). Together, this design allowed us to assess whether the retinotopic properties of face-selective regions vary across the visual field and with stimulus properties in a manner that could drive observed variations in our face recognition abilities.

Participants. Ten participants (six female, M_{age} = 29.1 years) took part, all of whom had normal or corrected-to-normal vision and gave written informed consent. Procedures were approved by the Experimental Psychology Research Ethics Committee at University College London.

Apparatus. Functional and anatomical scans were obtained using a Prisma 3T MRI scanner (Siemens, Erlangen, Germany). Stimuli were displayed on a back-projection screen in the bore of the magnet using an EPSON EB-L1100U projector that had a maximum luminance of 502 cd/m^2. The projector had a refresh rate of 60 Hz and a resolution of 1920 x 1200 pixels, with stimuli displayed in the central 1200 pixels (at a physical size of 27 x 27 cm). Participants viewed the screen through a mirror attached to the head coil at a viewing distance of 34 cm, giving a maximum field of view of 43.3° (±21.65° eccentricity). Gamma correction was performed, with the grey stimulus background presented at the mean projector luminance (251 cd/m^2).

Stimuli. Where prior work has examined the spatial selectivity of face-selective cortex by presenting one face at a time (Poltoratski et al., 2021), we developed totem-pole style bars of faces to more closely match the stimuli used for retinotopic mapping more broadly. While there is evidence that wedge-and-ring stimuli give pRF estimates with better

goodness-of-fit in V1 compared to bars (Alvarez et al., 2015), the use of wedge-and-ring stimuli requires eccentricity scaling to an extent that is unclear in face-selective regions. Instead we used bars, which have been shown to yield more accurate estimates of pRF eccentricity than wedge-and ring-stimuli (Linhardt et al., 2021). Where prior studies have examined only small regions of the visual field, here we wanted to cover a wider expanse of the visual field, particularly given the large sizes of pRFs in face-selective regions. Our bars thus covered a large field of view in length (43.3°; Figure 1A), with both horizontal and vertical orientations.

Stimuli were programmed using MATLAB (MathWorks, Inc) and PsychToolbox (Brainard, 1997; Pelli, 1997; Kleiner et al., 2007). Faces in each bar were selected from 15 male and 15 female faces, taken from the Radboud Face Database (Langner et al., 2010). Images were in colour and faces had a neutral expression. To maximise face-selective activation, we sought to minimise crowding between the faces (Louie et al., 2007; Kalpadakis-Smith et al., 2018), adaptation (Fang et al., 2007), and repetition suppression effects (Louie et al., 2007; Henson, 2016) by using faces with three viewpoints according to the view of the model: front- (90°), left- (135°) and right-facing (45°). This resulted in a total of 90 face images, which had their background removed and were resized to 332 x 450 pixels using Adobe Photoshop CS6. To further avoid adaptation/suppression effects tied to face identity (Natu et al., 2016), each identity could only appear once in a given bar. For the inverted face bars, faces were flipped along the vertical axis. The background of each bar matched the grey background of the experimental screen.

To ensure the visibility of faces in the periphery, and improve pRF fitting by maximally activating differently sized pRFs (both smaller pRFs near the fovea and larger pRFs peripherally), three bar widths were used – 5.3°, 7.0° and 10.1°. Face size was determined by the bar width (i.e. face sizes scaled with bar sizes). For each bar width, bar orientation (horizontal and vertical) and face orientation (upright or inverted), five bars containing male faces and ten bars containing female faces were generated (male bars appeared less frequently, as described below). Each bar contained faces of different viewpoints in a pseudo-randomised manner, such that faces of one viewpoint could not appear next to a face of the same viewpoint.

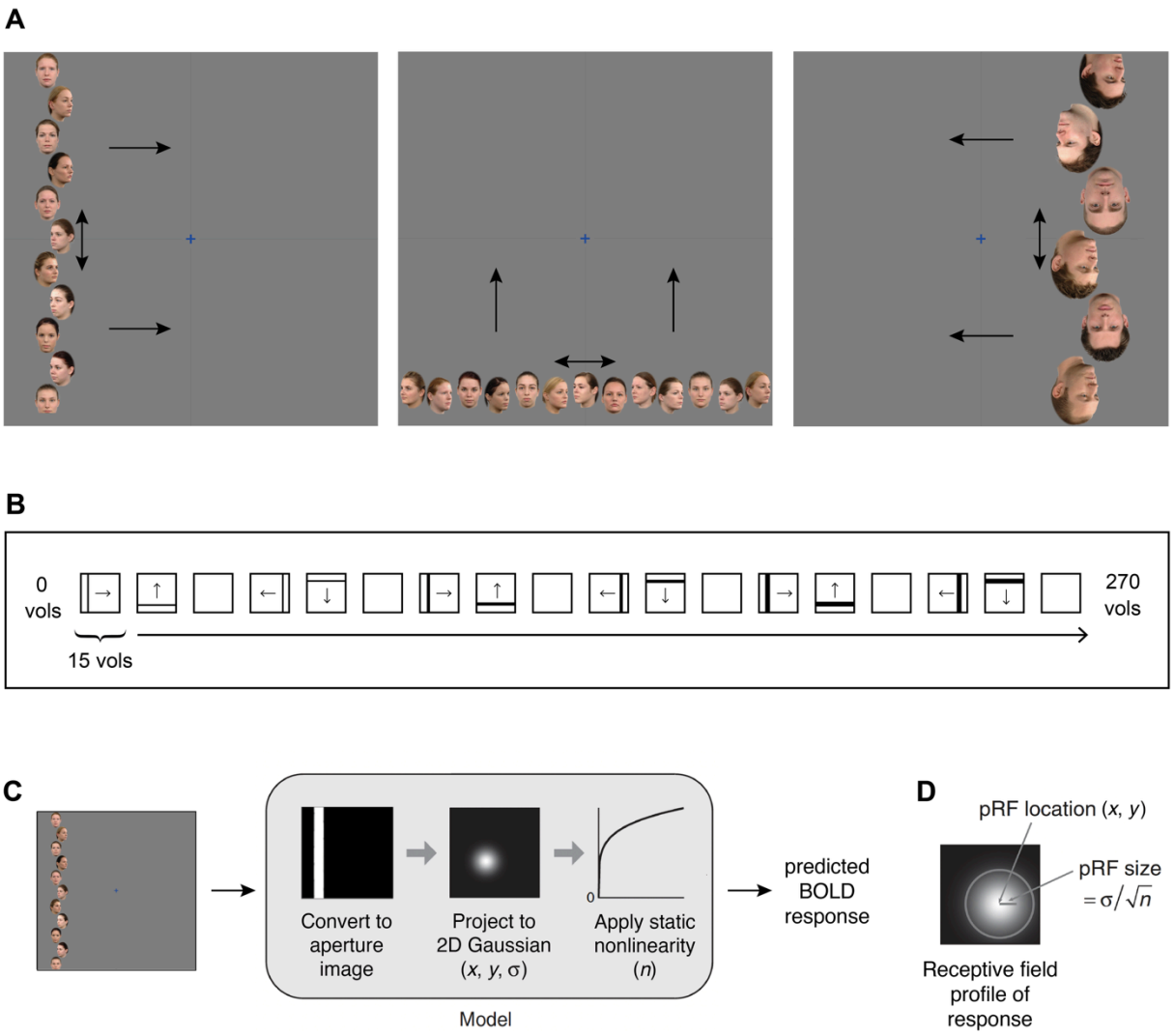

Figure 1. A. Example retinotopic mapping stimuli. A blue fixation cross appeared at the centre of the display while bars containing either male or female faces traversed the screen in one of four cardinal directions (shown by unidirectional arrows). Bars appeared at one location per TR (one second), moving back-and-forth along the length of the bar (shown by bidirectional arrows). Different bar widths and face orientations are shown in each panel. **B.** Bar conditions throughout the experiment. Each square represents one sweep across the screen (with 15 locations per sweep). The narrowest bars were shown first, proceeding to the widest. Blank periods (15 TRs) occurred after every two sweeps. Arrows represent the bars' direction of movement. **C.** pRF model. The stimulus was converted to a binary aperture image, with each pRF modelled as a 2D Gaussian before a static nonlinearity was applied using a compressive spatial summation parameter. The model output gives the predicted BOLD response. **D.** A depiction of pRF location and size in the compressive spatial summation model. Position is determined by *x* and *y* coordinates, while size is the standard deviation (σ) divided by the square root of the spatial summation exponent *n,* adapted from Kay et al., (2013).

To fill each bar, faces were shifted along the width of the bar (the x-axis for vertical bars and the y-axis for horizontal bars) so that they could be moved closer together along the opposite axis, reducing blank space. To further maximise the activation of

face-selective regions and ensure that the time-averaged bar locations contained faces in as much of the bar as possible, faces were moved along the length of the bar during presentation. To produce this motion, bars were made longer than required (varying from 49.08–57.32° depending on bar width and orientation) and then cropped to screen dimensions eight times along the longer axis, starting at a different point at equal increments along the bar. This resulted in eight differently cropped versions of each bar, played in sequence from the first to the eighth image and then back to the first for 66.7 ms each to give motion at a speed of 13.65, 17.63, or 25.59°/s (increasing with the width of the bars/faces). As such, faces within the bars moved smoothly side to side (horizontal bars) or up and down (vertical bars) at each location.

Procedure. Each run of the retinotopic-mapping procedure began with a blank screen for five seconds, with a central fixation cross subtending 0.95° of visual angle. Bars then stepped across the screen in four directions: 0° (rightwards), 90° (upwards), 180° (leftwards) and 270° (downwards), with one location per repetition time (TR), which lasted one second (Figure 1B). As above, faces moved along the length of the bar in each location to ensure that the time-averaged bar for each TR contained faces across the whole bar. Each sweep across the screen contained 15 equal steps, meaning that steps were smallest with the largest bar widths and vice versa. The number of steps was matched to avoid the pRF fitting being biased towards bar widths with more TRs (by contributing more to the least-squared error between data and model predictions used for model fitting). The thinnest bars were presented first (four sweeps, one per direction of motion) before moving on to the next thickness (Figure 1B). As there were three bar thicknesses, each run had a total of 12 sweeps. Every second sweep was followed by a blank period of 15 TRs. Each run therefore comprised 275 TRs (lasting 4 min. 35 sec.).

Participants were instructed to maintain fixation on a cross at the screen centre, whilst performing two tasks. To ensure fixation, participants were required to report when the fixation cross changed from blue to purple (0.002 probability, and lasting 0.2 seconds). To ensure that attention was directed towards the bars at the same time, participants were also required to respond when a bar containing male faces appeared in a given TR. Most bars contained female faces, while bars consisting of male faces occurred with 0.075

probability. Responses were recorded via a button box. Participants did not receive feedback, however key presses were monitored throughout the experiment to ensure that participants were engaging with the task. Upright and inverted runs were interleaved to avoid effects like fatigue disproportionately affecting one condition.

Localisation of face-selective ROIs. To identify face-selective Regions of Interest (ROIs), a functional localiser was run in the same scan session. In prior studies, these localisers have tended to use full-field stimuli presented foveally, with the subsequent investigation of spatial selectivity in face-selective regions then using stimuli presented only in the central 6-8° of the visual field. In scaling stimuli up to our 43.3° field of view, we were concerned that this approach would sub-optimally drive face-selective regions, given that large faces are less effective at engaging holistic processes (McKone, 2009). A second concern was that the use of full-field stimuli shown foveally may bias the localisation of face-selective regions towards voxels with a preference for large foveal stimuli, thereby exaggerating the extent of the foveal bias within face-selective regions.

For these reasons, we developed a novel localiser which presented faces and objects in both foveal and peripheral locations at a range of sizes. Images of faces, hands and instruments were displayed to cover the full 43.3° field of view. To maximise both foveal and peripheral stimulation, two configurations of stimuli were used: large, single images centred on the fovea, and smaller images tiled across the screen in a 3×3 grid (Figure S1). Similar to existing localisers (Stigliani et al., 2015; Schuurmans et al., 2023), faces, hands, and instruments were used as stimuli to isolate face-selective regions. Twenty images were created for each category, with contrast normalisation applied to give images a root mean square (RMS) contrast of 0.15. Twenty tiled images for each object category were then created by randomly selecting 9 images from the same category for the grid, ensuring that the same image did not appear twice. This gave 3 object categories (faces, hands, instruments) and 2 tiling conditions (single or tiled). In each case, images were shown on a noise background produced by iterative phase scrambling – each image (or image set) underwent a fast Fourier transform (FFT) followed by phase scrambling, pasting the faces/objects back onto this scrambled image, and scrambling again, with 500 repetitions (Petras et al., 2019).

Images from each of the 6 conditions were shown in blocks lasting 10 seconds each, with 20 stimuli from a given condition displayed one after the other for 500 ms each with no inter-stimulus interval. Single and tiled configurations were presented in the same run in separate blocks. Each run consisted of 51 blocks, with baseline (blank) periods for 10 seconds to begin and end, lasting 8 minutes and 50 seconds. Participants were instructed to maintain fixation and press a button when a phase-scrambled image appeared. Each participant completed two runs.

To identify face-selective brain regions we contrasted blood-oxygen-level-dependent (BOLD) responses to faces against the other object categories (Kanwisher et al., 1997; Weiner and Grill-Spector, 2010), combining both single and tiled versions (single and tiled faces > single and tiled hands, plus single and tiled instruments) using a general linear model (GLM) performed in SPM12 (Penny et al., 2011). Statistical contrasts were carried out using a threshold of $t \geq 2$, which was chosen to help maximise the number of pRFs remaining for further analyses after filtering by visual field location. We defined three face-selective areas (OFA, pFus and mFus; see Figure 2 for an example) in nine participants, though pFus could not be defined in one participant. Statistical T maps were surface projected using Freesurfer (Fischl, 2012) and used as a visual guide during the delineation of face-selective ROIs. Large areas were initially drawn manually, before an automatic process was used to define the ROI by identifying the vertex with the peak T statistic in each region and incorporating neighbouring vertices that were above the T threshold ($t \geq 2$). The inclusion of tiled images gave a significant increase in the vertices within each ROI compared to the use of single images alone (Figure S2).

MRI data acquisition. A 64-channel head coil was used with the 3T scanner, with cushions placed around participants' heads to minimise movement. Functional scans were run with only the back of the head coil, leaving 42 channels. A T1-weighted anatomical magnetisation-prepared rapid acquisition with gradient echo (MPRAGE) image was acquired (TR = 2300 ms and TE = 2.98 ms, voxel size = 1 mm isotropic voxels), along with functional T2-weighted multiband 2D echoplanar images (TR = 1000 ms, TE = 35.20 ms, voxel size = 2 mm isotropic voxels, 48 slices, flip angle = 60°, acceleration factor = 4). Each functional scan contained 270 volumes. A short 30 second localiser was carried out before

the functional scans and again before the anatomical scan, after the front head coil was fitted. Fixation was monitored throughout the experiment using an Eyelink 1000, although we did not record fixation data.

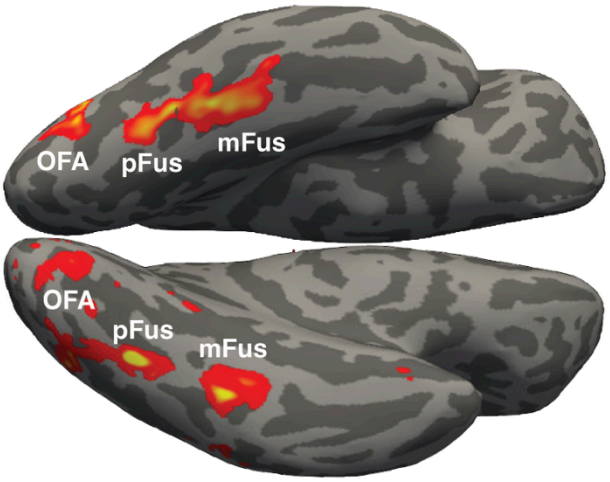

Figure 2. The location of face-selective ROIs (OFA, pFus, and mFus) on the ventral surface of an example participant's brain, as determined by statistical contrasts based on localiser runs.

MRI data preprocessing. For each participant, the T1 anatomical scan was automatically segmented and used to generate a 3D representation of the cortical surface using Freesurfer (Dale et al., 1999; Fischl et al., 1999; Fischl, 2012). Functional images were B0 distortion corrected and motion corrected using AFNI software (Cox, 1996). An alignment volume was created by finding the volume with the fewest voxel outliers across all runs, which all functional volumes were then aligned to. Using Freesurfer (Fischl, 2012), the alignment volume was co-registered to the structural image, and surface projection was performed.

pRF fitting. The four retinotopic-mapping runs were averaged and pRF analyses carried out using the SamSrf 9.4 MATLAB toolbox (Schwarzkopf, 2022). A Compressive Spatial Summation (CSS) model (Kay et al., 2013) was used within SamSrf 9.4 (Figure 1C), where each pRF was estimated as a two-dimensional Gaussian with a compressive non-linearity subsequently applied. This approach estimates pRF properties with a higher goodness-of-fit (R^2) compared to a linear pRF model, particularly in higher visual areas where responses to visual stimuli sum in a subadditive rather than linear manner (Kay et

al., 2013). The CSS model fitting involved four free parameters: *x* and *y* (the position of the pRF centre within the visual field), σ (the standard deviation or spatial spread of the pRF, in degrees of visual angle) and *n* (the exponent of the compressive non-linearity; Figure 1D). As the compressive nonlinearity affects the spread of the receptive field profile, during analyses we defined pRF size as σ divided by the square root of the exponent *n* (Kay et al., 2013). Stimulus locations were fed into model fitting via stimulus apertures created for each run, which were averaged across the four runs, resulting in one set of apertures comprising 270 frames (one for each TR). Because the faces moved within the bar stimuli (as described above), averaging these stimulus positions over time meant that the apertures formed solid bars, similar to standard retinotopic mapping procedures (Figure 1C).

The pRF fitting involved a coarse-to-fine approach. The coarse fit was carried out using an extensive multidimensional search space comprising 35,496 grid points, with different combinations of *x*, *y* and σ at each vertex. The parameters with the highest Pearson correlation between the predicted and observed time series were then selected. These values were used to seed the fine fit, which used the Nelder-Mead simplex-based method (Nelder and Mead, 1965) to reduce the residual sum of squares (RSS) between the predicted and observed time series, and determine optimal values for the four free parameters (*x*, *y*, σ, and *n*).

Delineation of early visual areas. Prior to delineation, vertices with a goodness-of-fit threshold below 0.2 were removed, and a smoothing kernel of 3 mm full width half maximum (FWHM) was applied. pRF locations (*x* and *y*) were used to project colour-coded polar angle and eccentricity maps onto the cortical surface (Figure 3). Visual areas V1-V3 were delineated using an auto-delineation tool and then corrected manually using SamSrf 9.4 (Schwarzkopf, 2022). This involved using standard criteria based on reversals in polar angle (DeYoe et al., 1994; Sereno et al., 1995; Engel et al., 1997), assisted by the eccentricity maps. These early regions were delineated using the maps for the upright face condition, before being checked and corrected (if needed) using the inverted maps to ensure correspondence between the two. Face-selective areas were delineated via localiser analyses, as above.

Vertex selection. To avoid artefacts, vertices that had beta amplitudes of less than 0.01 or greater than 3 (*z* scores), sigma values of 0, or which were located perfectly at the centre (*x* and *y* of exactly 0, indicative of fitting errors) were removed. To avoid noisy and unreliable vertices, those with a goodness-of-fit threshold (R^2) below 0.2 were also removed (as above). In OFA and mFus, some participants showed vertices with very low pRF size estimates (almost 0) at high eccentricities, which upon closer analysis were the result of poor fits. To avoid these unreliable estimates affecting the main pattern of results, we increased the R^2 threshold within face-selective ROIs for some participants (OFA: four participants = 0.4, mFus: one participant = 0.4, one participant = 0.3).

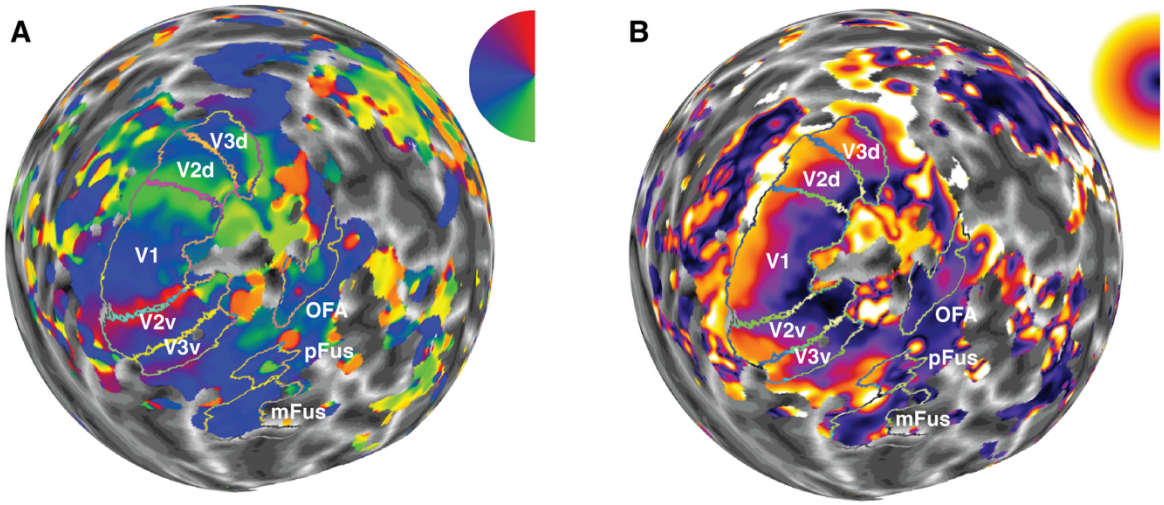

Figure 3. Example retinotopic maps from one participant. **A.** A polar angle map plotted on an inflated, spherical cortical surface (right hemisphere), with delineations of V1-V3 and OFA, pFus and mFus outlined. The colour wheel indicates polar angle coordinates (green for the lower visual field, blue around the horizontal meridian, red for the upper field). **B.** An eccentricity map for the same participant, where purple represents central eccentricities and yellow more peripheral locations.

Location analyses. To compare pRF properties across the visual field, pRFs were filtered according to their centre position. Four wedges were defined, each including polar angle locations within ±45° on either side of the left horizontal, right horizontal, upper vertical and lower vertical meridians. Although behavioural research has suggested that visual field anisotropies decline at locations more than 30° away from the meridian (Abrams et al., 2012; Benson et al., 2021), fMRI studies that used a wedge-based approach have shown that asymmetries in cortical surface were similar across different wedge widths (Himmelberg et al., 2023b), and that anisotropies in pRF properties could be

found using 45° wedges (Silva et al., 2018). In our data, patterns were similar regardless of whether the wedge width was 30° or 45°. We thus used the wider wedge width of 45° given that it considerably increased the number of pRFs remaining after filtering. For horizontal-vertical comparisons, the left and right wedges were combined to make the horizontal meridian, with upper and lower wedges combined to make the vertical meridian.

Visual field coverage. Visual field coverage was calculated by generating a Gaussian receptive field profile for each vertex based on its centre position (*x,y*), eccentricity and sigma (σ), and then raising the receptive field profile by the spatial summation exponent (*n*), matching the best-fitting CSS model. Receptive field profiles were then summed across vertices to give coverage values across the visual field for each ROI, face orientation (upright/inverted), and participant. Because absolute values would differ based on numerous factors (e.g. the number of vertices, sigma values, and exponents), we normalised coverage values by dividing by their maximum value across both upright and inverted maps (separately for each ROI and participant). Coverage therefore represents the proportion of the peak response (within each ROI) at each visual field location. Coverage values were extracted from these plots according to eccentricity and polar angle location (using the wedges described above) for further analyses. Note that our approach differs from prior studies where coverage has been calculated using binary circles (e.g. Witthoft et al., 2016; Poltoratski et al., 2021). Although these binary approaches incorporate the position and size of receptive fields, they do not capture the spatial profiles of the constituent pRFs. By summing the profiles, we aimed to better account for the spatial pattern of responsiveness within each pRF when generating estimates of coverage.

Statistical analyses. We were interested in three pRF properties: size ($\sigma\sqrt{n}$), number (the total amount of pRFs after poor-fitting vertices were removed) and visual field coverage (the values extracted from the coverage plots). These properties were examined in eccentricity bins of 1° width, ranging from from 0.5° to 21.5°.

Linear mixed effects models were used to investigate whether location, inversion and eccentricity could predict pRF size. Because the location of each pRF was determined

by its centre, size could not be estimated if there were no pRF centres within that region. Linear mixed models can deal with these 'missing' estimates by examining the linear change in pRF size with eccentricity. Separate mixed effects models were run for each ROI (V1, V2, V3, OFA, pFus, and mFus). Our main analyses examined pRF size with fixed factors for visual field location (horizontal/vertical or upper/lower), eccentricity and inversion (upright/inverted), with a second analysis examining fixed factors for eccentricity and inversion (upright/inverted) irrespective of location. Participant was specified as a random factor for the intercept as well as for each of the fixed factors, as the slope of the relationship between pRF size and eccentricity, location and/or inversion could vary across individuals. Differences at each eccentricity were then examined using Wilcoxon signed rank tests.

Because pRF number and visual field coverage showed non-linear profiles, mixed effects analyses of variance (ANOVAs) were used to assess the effects of eccentricity, inversion, location and participant on these properties. Separate ANOVAs were run for each ROI (V1, V2, V3, OFA, pFus and mFus). Our main analyses included within-subjects fixed factors for location, eccentricity, and inversion (upright/inverted), with a second analysis run to examine effects of inversion regardless of location. In all ANOVAs, participant was entered as a between-subjects random factor. Inversion effects and location differences were then examined via t-tests or Wilcoxon signed rank tests (if sphericity or homoscedasticity assumptions were violated).

Results

We used population receptive field (pRF) mapping to compare the spatial selectivity of early visual cortex (V1-V3) with three face-selective regions of ventral occipitotemporal cortex (OFA, pFus, mFus). Best-fitting parameters for the CSS model gave a good characterisation of the BOLD responses to our stimuli, with high average R^2 values and equivalent levels with both upright and inverted face stimuli (Figure S2A). Consistent with prior work (Kay et al., 2013; Poltoratski et al., 2021), the exponent of the compressive non-linearity (the *n* parameter) averaged below 1 in all regions tested (indicating a

compressive nonlinearity), and decreased in the higher face-selective regions of the visual hierarchy (Figure S2B). Maps of the full visual field coverage for each ROI are displayed in Figure S3, separately for upright and inverted faces. All ROIs showed some degree of coverage throughout the visual field, including at the farthest eccentricities tested, though a bias towards foveal locations is also evident, particularly in face-selective regions. While coverage patterns are similar regardless of face orientation in early visual cortex, in mFus there is broader coverage in both peripheral and central locations for upright vs. inverted faces.

We first assessed how retinotopic properties (pRF size, number, and visual field coverage) differed according to polar angle, and in particular whether variations in this *spatial selectivity* follow the expected anisotropies along the horizontal vs. vertical meridian and in the upper vs. lower field. As we observed similar location-based variations in these measures for upright and inverted faces, the following sections on visual field anisotropies discuss the results for upright faces only. We then examined whether variations in these retinotopic properties might also subserve the *stimulus selectivity* of face perception for upright rather than inverted faces.

Visual field anisotropies

pRF size

Consistent with prior work, pRF size increased throughout the visual hierarchy, averaging 1.1° in V1, 1.6° in V2, 2.8° in V3, and then 6.2° in OFA, 7.5° in pFus and 8.2° in mFus. Sizes also increased with eccentricity in all visual regions, as shown in Figure 4. We first compared the horizontal and vertical meridians (Figure 4A). In early visual cortex, pRF sizes did not differ significantly along the horizontal and vertical meridians in V1 (β = 0.13 [-0.16, 0.44], p = .373) nor V2 (β = -0.01 [-0.38, 0.36], p = .953), contrary to predictions. A main effect of location was found in V3 (β = 0.79 [0.17, 1.41], p = .012), with Wilcoxon tests indicating that pRFs were significantly larger along the vertical than horizontal meridian at eccentricities from around 5-15° (see lines in Figure 4A), consistent with the pattern predicted by behavioural anisotropies. In face-selective regions, the number of pRFs in the periphery dropped markedly along the vertical meridian (to be discussed below regarding

pRF number), meaning that size estimates were missing at many eccentricities. However, pRF sizes did not differ significantly between the horizontal and vertical meridian in any of these areas, neither for the OFA (β = -0.48 [-2.05, 1.10], p = .551), pFus (β = 0.24 [-1.15, 1.63], p = .734) nor mFus (β = 1.22 [-0.10, 2.54], p = .070).

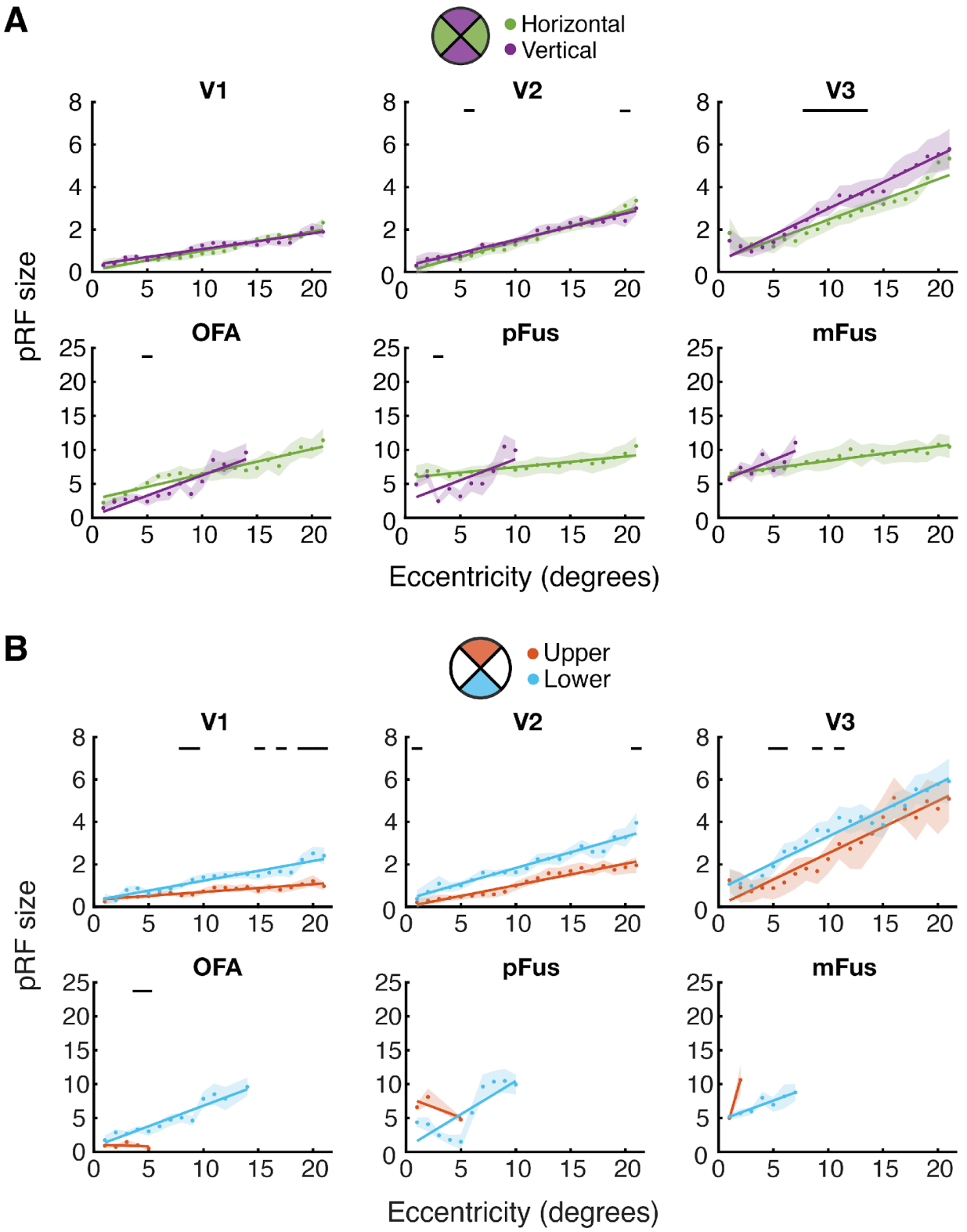

Figure 4. Mean pRF size measured with upright faces across eccentricity along the horizontal (green) and vertical (purple) meridians **(A)** and in the upper and lower visual field **(B)**. At each eccentricity, size estimates were only plotted if they were averaged from at least five vertices. Black lines indicate significant differences at each location ($p < .05$).

Figure 4B plots the comparison of pRF sizes in the upper and lower fields. In early visual cortex, pRFs were larger in the lower than the upper field, with significant main effects of location (V1: β = 0.66 [0.20, 1.13], p = .006; V2: β = 0.88 [0.16, 1.61], p = .017; V3: β = 0.84 [0.06, 1.62], p = .035) and significant t-tests across a range of eccentricities. These differences run in the opposite direction to that predicted by behavioural anisotropies, given that performance is typically worst in the upper field. In face-selective regions, there was also an effect of location in OFA (β = 2.30 [0.94, 3.67], p = .001), with pRFs again larger in the lower vs. upper field. Size estimates did not differ significantly between the upper and lower field in pFus (β = -0.72 [-4.27, 2.83], p = .689) or mFus (β = -1.72 [-3.76, 0.31], p = .096). Taken together, these findings suggest that pRF size was not consistently modulated by location in a manner consistent with behavioural anisotropies, either in early visual cortex or face-selective regions. Estimates of pRF size obtained with inverted face stimuli show similar patterns of variation (Figure S4).

pRF number

We next examined variations in the number of pRFs in each region (after filtering by R^2, beta, and sigma thresholds). As in prior work, the number of pRFs decreased with eccentricity in all visual areas (Figure 5). The number of pRFs also decreased moving up the hierarchy, with lower numbers evident in face-selective areas and more dramatic reductions in pRF number in the periphery, consistent with a magnified foveal bias in these regions compared to early visual cortex.

Figure 5A plots pRF numbers along the horizontal and vertical meridians, which show clear differences in early visual cortex. The main effect of location was significant in V1 ($F_{1,180}$ = 26.83, p < .001) and V3 ($F_{1,180}$ = 224.16, p < .001) driven by the greater number of pRFs on the horizontal meridian. Although there was no main effect of location in V2 ($F_{1,180}$ = 0.01, p = .957), all three areas show a clear drop in pRF numbers on the vertical meridian with eccentricity, increasing the horizontal-vertical difference. Significant interactions between location and eccentricity were indeed evident in each case (V1: $F_{20,180}$ = 14.64, p < .001; V2: $F_{20,180}$ = 16.54, p < .001, V3; $F_{20,180}$ = 7.94, p < .001). Wilcoxon tests showed that all three early visual areas had significantly more pRFs along the horizontal

than vertical meridian in peripheral vision, with significant differences over a greater proportion of the visual field in V3 compared to V1 and V2. In face-selective cortex, a strong foveal bias was evident in all three areas, with pRF numbers dropping markedly at eccentricities beyond 5-10°. All three face-selective regions nonetheless show greater pRF numbers along the horizontal than vertical meridian, confirmed by main effects of location in each (OFA: $F_{1,180}$ = 16.49, p = .003; pFus: $F_{1,160}$ = 15.92, p = .004, mFus; $F_{1,180}$ = 7.27, p = .025). There were again interactions between location and eccentricity in all three regions (OFA: $F_{20,180}$ = 15.86, p < .001; pFus: $F_{20,160}$ = 7.81, p < .001, mFus; $F_{20,180}$ = 6.53, p < .001), though here Wilcoxon tests reveal significant differences both near the fovea and in the periphery. This over-representation of the horizontal meridian follows the predicted direction for behavioural anisotropies in both early and face-selective cortex.

Figure 5B plots differences in the lower vs. upper field, where main effects of location in V1-V3 confirmed a greater number of pRFs in the lower field, as predicted by behavioural anisotropies (V1: $F_{1,180}$ = 36.19, p < .001; V2: $F_{1,180}$ = 34.59, p < .001, V3; $F_{1,180}$ = 10.37, p = .011). Interactions between location and eccentricity were also significant (V1: $F_{20,180}$ = 3.86, p < .001; V2: $F_{20,180}$ = 7.45, p < .001, V3; $F_{20,180}$ = 2.68, p < .001), with Wilcoxon tests showing that the upper-lower difference generally increased towards the periphery. Upper-lower differences in pRF number were even more pronounced in face-selective regions, with all three face-selective areas showing strikingly few pRFs in the upper field. This gave main effects of location in OFA ($F_{1,180}$ = 7.87, p = .021) and mFus ($F_{1,180}$ = 19.06, p = .002), with more pRFs in the lower than upper field, consistent with predictions. Although there was no main effect of location in pFus ($F_{1,160}$ = 2.93, p = .125), the interaction between location and eccentricity was significant for all three areas (OFA: $F_{20,180}$ = 5.05, p < .001; pFus: $F_{20,160}$ = 2.92, p < .001; and mFus: $F_{20,180}$ = 11.29, p < .001). Wilcoxon tests showed that upper-lower differences were more pronounced near the fovea in OFA. Although the Wilcoxon tests did not find significant upper-lower differences in pFus and mFus, this is likely related to the low number of pRFs along the vertical meridian in these regions. Estimates of pRF number obtained with inverted face stimuli show similar patterns (Figure S5). Together, we observe more pRFs along the horizontal vs. vertical

meridian and in the lower vs. upper field across both early and face-selective brain regions, in a manner consistent with behavioural anisotropies.

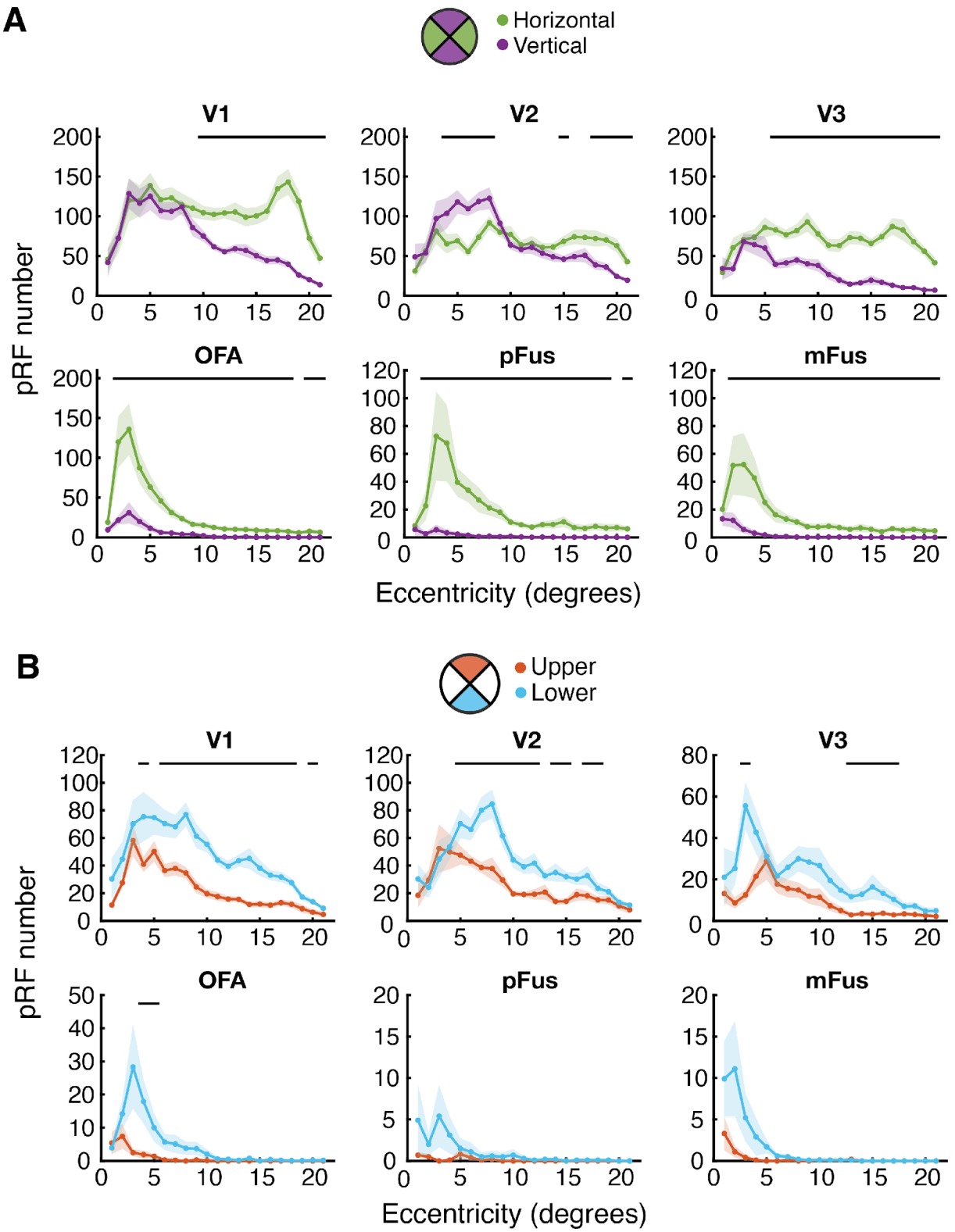

Figure 5. The mean number of pRFs responsive to upright face bars, plotted as a function of eccentricity along the horizontal (green) and vertical (purple) meridians **(A)** and in the upper and lower visual field **(B)**. Black lines indicate significant differences at each location ($p < .05$).

Visual field coverage

Although the above variations in pRF size and number are somewhat mixed, we can examine their joint operation by computing pRF coverage around the visual field. Figure 6 plots the resulting coverage values separated by visual field location. Each brain region shows some degree of coverage throughout the periphery, though there is a clear decline with eccentricity, most rapidly in face-selective areas. Comparing the horizontal and vertical meridians in early visual cortex (Figure 6A), there were significant main effects of location in all three areas (V1: $F_{1,180} = 8.36$, $p = .018$; V2: $F_{1,180} = 9.32$, $p = .014$; V3: $F_{1,180} = 46.57$, $p < .001$), driven by higher coverage along the horizontal compared to the vertical meridian, consistent with the pattern of behavioural variations. There were also significant interactions between location and eccentricity in all three regions (V1: $F_{20,180} = 30.78$, $p < .001$; V2: $F_{20,180} = 31.70$, $p < .001$; V3: $F_{20,180} = 59.97$, $p < .001$), given that horizontal-vertical differences were most evident at intermediate eccentricities. Across early visual cortex, t-tests revealed differences at the majority of eccentricities tested, with the horizontal-vertical anisotropy becoming particularly pronounced in V3 relative to the earlier areas.

Face-selective brain regions all showed small but consistent horizontal-vertical anisotropies in visual field coverage, again with greater coverage on the horizontal meridian and significant main effects of location in all three areas (OFA: $F_{1,180} = 11.84$, $p = .007$; pFus: $F_{1,160} = 7.20$, $p = .028$; mFus: $F_{1,180} = 14.94$, $p = .004$). There were also interactions between location and eccentricity in OFA ($F_{20,180} = 3.17$, $p < .001$) and pFus ($F_{20,160} = 8.67$, $p < .001$) but not in mFus ($F_{20,180} = 0.27$, $p = .999$). t-tests showed that these horizontal-vertical differences were present across most eccentricities in pFus, and all of them in OFA and mFus (the latter being small but nonetheless consistent). Altogether, these results reveal a consistent horizontal-vertical difference across the visual field within face-selective cortex, in a direction consistent with behavioural anisotropies.

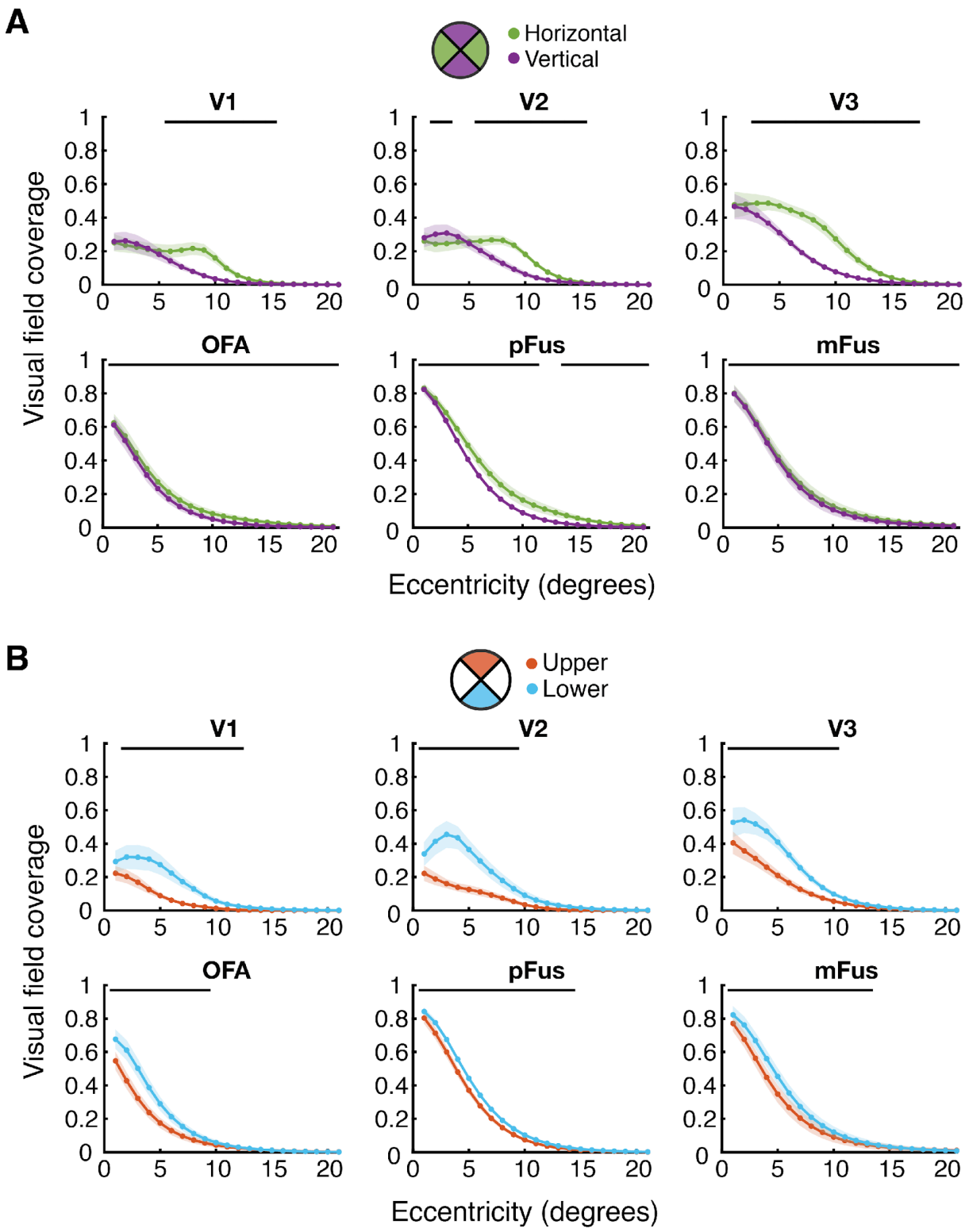

Figure 6. Mean visual field coverage across eccentricity along the horizontal (green) and vertical (purple) meridians **(A)** and in the upper and lower visual field **(B)**. Black lines indicate significant differences at a given location ($p < .05$).

Coverage also differed in the upper vs. lower field throughout V1-V3, with higher coverage in the lower vs. upper field, again consistent with behavioural effects. The main effect of location was accordingly significant in all areas (V1: $F_{1,180} = 25.67$, $p < .001$; V2: $F_{1,180} = 31.87$, $p < .001$; V3: $F_{1,180} = 19.72$, $p = .002$). All three regions showed significant interactions between location and eccentricity (V1: $F_{20,180} = 30.79$, $p < .001$; V2: $F_{20,180} = 51.05$, $p < .001$; V3: $F_{20,180} = 32.37$, $p < .001$), with t-tests confirming significant upper-lower differences only for eccentricities below 10°. Face-selective regions also had greater visual field coverage in the lower vs. upper field, shown by main effects of location in all three areas (OFA: $F_{1,180} = 16.09$, $p = .003$; pFus: $F_{1,160} = 10.32$, $p = .012$; mFus: $F_{1,180} = 24.80$, $p < .001$). Like early visual cortex, there were also interactions between location and eccentricity (OFA: $F_{20,180} = 41.28$, $p < .001$; pFus: $F_{20,160} = 13.21$, $p < .001$; mFus: $F_{20,180} = 18.49$, $p < .001$), with t-tests again revealing significant differences at eccentricities below 10-15° but not beyond. Estimates of visual field coverage obtained using inverted face stimuli show similar patterns (Figure S6).

In sum, coverage was consistently higher along the horizontal than vertical meridian and in the lower than upper field in both early visual cortex and face-selective areas. These variations in coverage, along with those for pRF number, demonstrate that low- and high-level visual areas show the same anisotropies in visual field sampling. This commonality does not however extend to pRF size, which showed more variable patterns that are less able to explain behavioural anisotropies.

Inversion

Given that the spatial properties of both early and face-selective cortex vary in a manner consistent with behavioural anisotropies, these properties may also vary with face orientation, following suggestions that smaller pRFs drive the advantage for upright over inverted face recognition (Poltoratski et al., 2021). During scans, to ensure that we engaged these face-selective processes, participants performed a gender recognition task. Performance showed a clear advantage for upright faces (Figure S7A), replicating the well-established inversion effect (Yin, 1969; Rossion and Gauthier, 2002) and demonstrating that our task was sufficient to engage configural face-recognition

processes. This difference in difficulty did not affect fixation, with performance on the concurrent colour-change task at fixation equivalent with upright and inverted faces (Figure S7B).

pRF properties were examined for upright vs. inverted faces, here regardless of visual field location (i.e. pooling across the whole field). These properties did not differ in early visual cortex, as one would expect given the lack of selectivity for face orientation (shown in Figure S8). We focus instead on face-selective regions. Previous work has reported larger pRFs for upright compared to inverted faces in mFus and pFus but not OFA (Poltoratski et al., 2021). Here we observe larger pRFs for *inverted* than upright faces in OFA (Figure 7A), with a significant main effect of inversion (β = 0.97 [0.32, 1.61], p = .003). In pFus, pRF sizes were similar in both upright and inverted conditions, with a non-significant main effect (β = 0.32 [-0.46, 1.11], p = .416). This was also the case in mFus – despite a trend towards larger pRFs in the periphery for upright faces, the main effect of inversion was non-significant (β = -0.58 [-2.45, 1.28], p = .538). Wilcoxon tests further showed only sporadic significant differences with inversion at specific eccentricities within the three areas. As with the location variations discussed above, we conclude that pRF size was not modulated by inversion in a consistent manner.

For pRF number (Figure 7B), there were no main effects of inversion in any of the face-selective regions (OFA: $F_{1,180}$ = 0.24, p = .634; pFus: $F_{1,160}$ = 2.48, p = .154; mFus: $F_{1,180}$ = 0.53, p = .484). However, there were significant interactions between inversion and eccentricity in all three areas (OFA: $F_{20,180}$ = 2.69, p < .001; pFus: $F_{20,160}$ = 1.97, p = .011; mFus: $F_{1,180}$ = 1.72, p = .034). Wilcoxon tests did not find consistent upright-inverted differences in OFA and pFus. In mFus, there were significantly more pRFs for upright vs. inverted faces over the majority of eccentricities outside of the fovea (despite one eccentricity near the fovea with more pRFs for inverted faces). This variation in the number of pRFs in mFus thus largely follows a pattern that could drive the behavioural Face Inversion Effect.

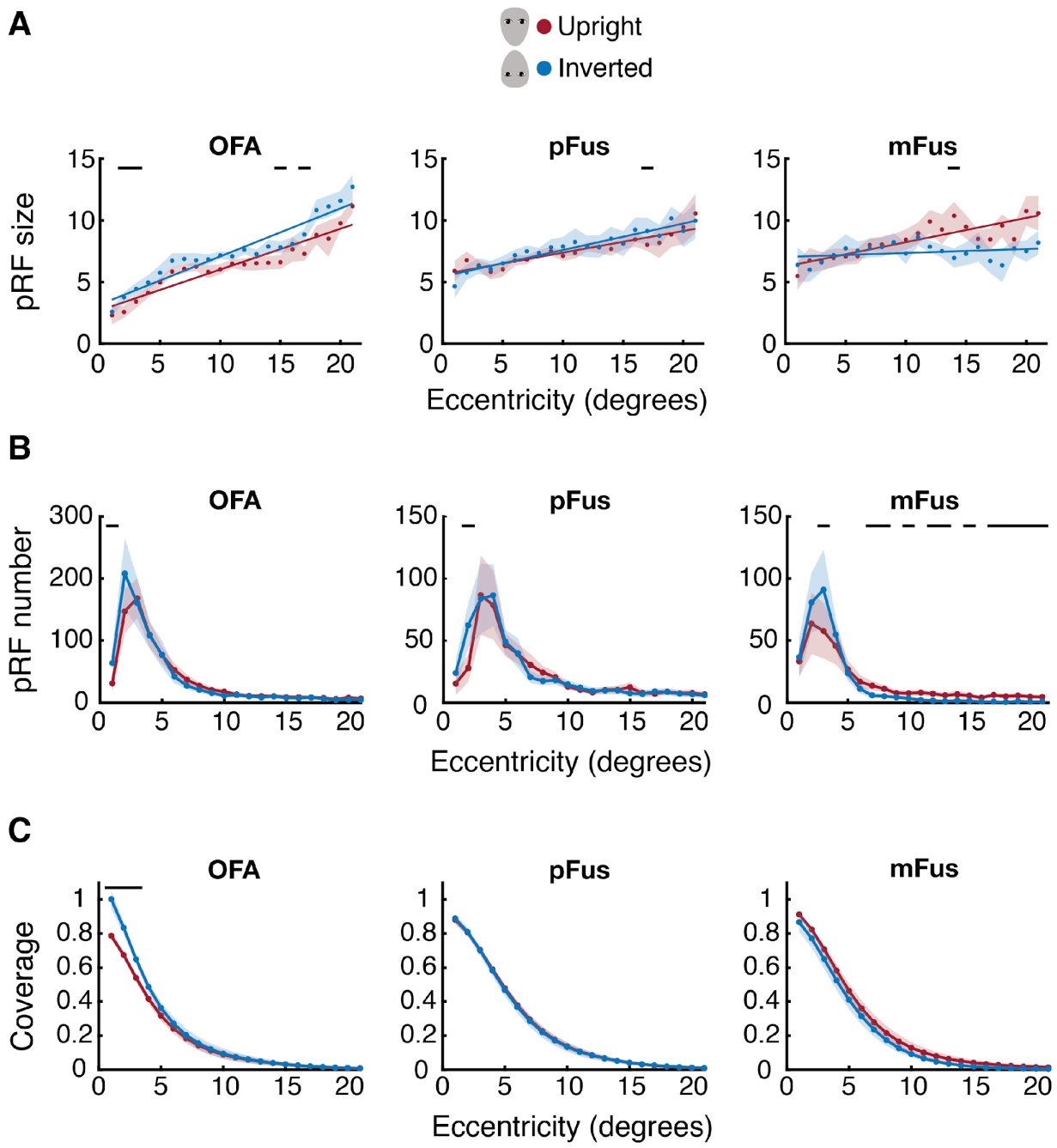

Figure 7. The effect of face orientation on spatial selectivity in face-selective regions, plotting mean pRF size **(A)**, pRF number **(B)** and visual field coverage **(C)** across eccentricity for upright (red) and inverted (blue) faces, separately in the OFA, pFus and mFus. Black lines indicate significant differences in each property according to face inversion ($p < .05$).

Finally, estimates of visual field coverage (Figure 7C) were higher near the fovea for inverted vs. upright faces in OFA, though the main effect of inversion was non-significant ($F_{1,180} = 0.02$, $p = .884$), as was the interaction between inversion and eccentricity ($F_{20,180} = 0.97$, $p = .496$). These effects were similarly non-significant in pFus, both for the main

effect ($F_{1,160}$ = 0.13, p = .731) and interaction ($F_{20,160}$ = 0.31, p = .998). Although the pattern seen in OFA reversed in mFus to give slightly higher coverage levels across the visual field for upright vs. inverted faces, the main effect ($F_{1,180}$ = 2.18, p = .174) and interaction with eccentricity ($F_{20,180}$ = 1.00, p = .460) were both non-significant. The lack of variation in coverage with face inversion suggests that this property could not drive differences in performance with upright vs. inverted faces, nor do we see evidence that pRF sizes differ reliably across these conditions, as above. Variations in the number of pRFs sensitive did nonetheless follow the expected pattern in mFus, with greater numbers of pRFs found to be responsive to upright vs. inverted faces.

Discussion

We show that the spatial selectivity of face-selective cortex (OFA, pFus, and mFus) follows the same anisotropic pattern of variations evident in earlier retinotopic areas (V1-V3). In all of these areas, we observe a greater *number* of population receptive fields (pRFs) and higher *visual field coverage* along the horizontal vs. vertical meridian and in the lower vs. upper field. These common variations suggest a continuity of visuospatial coding in the visual system, where high-level category-selective cortex encodes objects using the same spatial framework established in early regions (Groen et al., 2022). This pattern is also consistent with the behavioural anisotropies observed for both low-level vision (Carrasco et al., 2001; Abrams et al., 2012; Greenwood et al., 2017; Barbot et al., 2021; Himmelberg et al., 2023a) and higher-level face perception (Roux-Sibilon et al., 2023; Morsi et al., 2024). In contrast, *pRF sizes* did not vary in a consistent manner across the visual field in either early or face-selective regions, suggesting this property is poorly suited to explain the observed behavioural anisotropies. Similarly, neither pRF sizes nor coverage varied with the orientation of faces, contrary to prior reports (Poltoratski et al., 2021). We did however observe a reduction in pRF number in mFus for inverted relative to upright faces, suggesting that similar principles could underlie both the spatial and stimulus selectivity in face-selective regions.

In early visual cortex, our observation of greater pRF numbers and increased visual field coverage along the horizontal vs. vertical meridian and in the lower vs. upper field is consistent with previous findings (Amano et al., 2009), as well as prior demonstrations of greater cortical magnification and surface area in these locations (Silva et al., 2018; Himmelberg et al., 2023b). Here we report that these variations also arise in face-selective regions – OFA, pFus and mFus all showed these same variations in pRF number and coverage (though the upper-lower difference in pRF number did not reach significance in pFus). In each case, horizontal-vertical differences were more pronounced than the upper-lower differences, consistent with behavioural studies showing that the upper-lower difference is smaller in magnitude in both low-level vision (Greenwood et al., 2017; Barbot et al., 2021; Kurzawski et al., 2021) and for face perception (Morsi et al., 2024).

As in prior studies, we also observe a marked increase in the foveal bias in face-selective regions (Kay et al., 2015; Finzi et al., 2021; Poltoratski et al., 2021; Silson et al., 2022), whereby the drop in pRF number with eccentricity became increasingly steep relative to early visual cortex. The preservation of the horizontal-vertical and upper-lower anisotropies in these regions despite these changes suggests that these anisotropies are actively maintained in category-selective cortex, rather than being passively inherited from the variations in early cortex. This active maintenance may reflect a drive in sensitivity towards the typical locations of faces in the visual field – for instance, the bias towards the horizontal meridian may reflect people generally being of a similar height, meaning that we often encounter faces along the horizontal plane (de Haas et al., 2016). Similar principles are evident elsewhere in category-selective cortex, where the retinotopic properties of scene-selective areas show a reversed upper-lower anisotropy, matching the upper-field advantage in scene-recognition tasks (Silson et al., 2015).

Despite the sharp reductions in the number of pRFs centred on peripheral vision, some degree of visual field coverage remained across all eccentricities tested (up to ±21.65°) within face-selective areas. This level of visual field coverage is sufficient to support the clear face-recognition abilities observed in peripheral vision (McKone, 2004; Kovacs et al., 2017; Kalpadakis-Smith et al., 2018; Roux-Sibilon et al., 2023; Morsi et al., 2024), as well as to detect and direct rapid saccades towards peripheral face stimuli

(Crouzet et al., 2010; Boucart et al., 2016), though some decline in efficiency is nonetheless apparent when peripheral recognition is compared to foveal vision (Mäkelä et al., 2001). This peripheral coverage is driven by the large receptive fields in face-selective areas, which can thus be seen as an adaptive response to the reduced neural representation of the periphery.

Our results do not offer support for a common pattern of anisotropies in pRF size through the visual hierarchy. Though area V3 showed the expected horizontal-vertical difference of larger pRFs along the vertical than horizontal meridian, these differences were not observed in V1 and V2. We also found *larger* pRFs in the lower than upper field across early visual cortex, the opposite direction to that predicted by behavioural anisotropies. This is consistent with prior reports of little-to-no difference in pRF sizes along the vertical meridian in particular (Himmelberg et al., 2023b), though differs from studies reporting a horizontal-vertical difference across V1-V3 (Silva et al., 2018) and smaller pRFs in the lower vs. upper field (Silson et al., 2018; Silva et al., 2018). These mixed findings may in part reflect the inherent variability in measurements of pRF size, which are known to be more susceptible to variations in stimulus properties, attention, or fitting procedures than properties like pRF location (Alvarez et al., 2015; van Dijk et al., 2016). Nonetheless, the lack of variation in pRF sizes for face-selective regions in our dataset consolidates these mixed findings in early visual cortex, suggesting that receptive field size is not the main factor driving differences in perception across the visual field.

The size of face-selective pRFs was also invariant to face orientation, contrary to prior results (Poltoratski et al., 2021). In addition to the above-noted challenges in measuring pRF size, these previously observed reductions may reflect their reduced beta amplitudes for inverted vs. upright faces, which can reduce goodness-of-fit (Schwarzkopf et al., 2014; Anderson et al., 2017), in turn biasing averages towards smaller values since larger pRFs tend to drop out first (Alvarez et al., 2015; Hughes et al., 2019). This effect is absent in our results, given similar beta amplitudes for upright and inverted faces (Figure S2C). We nonetheless found a clear behavioural inversion effect (Figure S7), confirming the engagement of face-specific processes during scans. More broadly, the invariance in pRF size with inversion and visual field location together challenge the association between

larger receptive fields and better face recognition (Witthoft et al., 2016; Avidan and Behrmann, 2021). Further evidence against this theory is our observation that pRF size increases with eccentricity within face-selective regions, as in prior studies (Kay et al., 2013; Poltoratski et al., 2021). If larger pRFs improved recognition, performance should improve in peripheral vision, contrary to published findings (Mäkelä et al., 2001; McKone, 2004). Together these findings suggest that the inversion effect cannot be explained by changes in pRF size.

We do however observe a greater number of pRFs for upright than inverted faces in area mFus, particularly in the periphery. Changes in the number of face-selective neurons with inversion could therefore drive the differences in these abilities, consistent with the reduced BOLD signal with inversion in face-selective regions (Kanwisher et al., 1998). The greater number of responsive voxels for upright faces may reflect the recruitment of neurons selective for the configural properties and/or natural statistics of upright faces (Le Grand et al., 2001; Rossion, 2008). This partly aligns with the variation in pRF numbers around the visual field (though without a corresponding increase in coverage for upright faces), suggesting some overlap between the spatial and stimulus selectivity of face-selective cortex. However, the inversion-related differences in pRF number were smaller than the variations across the visual field, despite the robust behavioural inversion effect and its consistency in prior work. It remains possible that the inversion effect also reflects qualitative differences in the firing of face-selective neurons, rather than purely quantitative differences in the number of active neurons.

Altogether our results demonstrate that face-selective cortex differentially samples the visual field in a similar fashion to early visual cortex, with greater pRF numbers and better visual field coverage along the horizontal vs. vertical meridian and in the lower vs. upper field. These retinotopic variations are consistent with the behavioural anisotropies found in both low-level vision (Carrasco et al., 2001; Abrams et al., 2012; Greenwood et al., 2017; Barbot et al., 2021; Himmelberg et al., 2023a) and face perception (Roux-Sibilon et al., 2023; Morsi et al., 2024). In contrast, variations in pRF size did not reliably follow the same pattern as these behavioural anisotropies in either early or face-selective regions. Although large receptive fields are likely necessary to support face-recognition abilities in

peripheral vision, given the magnified foveal bias in face-selective regions, variations in size do not appear to drive variations in these abilities. Given that pRF numbers in area mFus also decrease with face inversion, at least some of the stimulus selectivity within face-selective brain regions can be understood using similar principles to the spatial selectivity in these regions. More broadly, the common spatial selectivity in early visual cortex and specialised face-selective regions supports proposals (Groen et al., 2022) for a shared visuospatial framework throughout the visual system.

Acknowledgements

Funded by the Biotechnology and Biological Sciences Research Council [BB/J014567/1]. Thanks to Jolien Schuurmans for supplying stimuli used in the functional localiser for face-selective brain regions.

Conflicts of interest

The authors declare no competing financial interests.

Supplementary Information

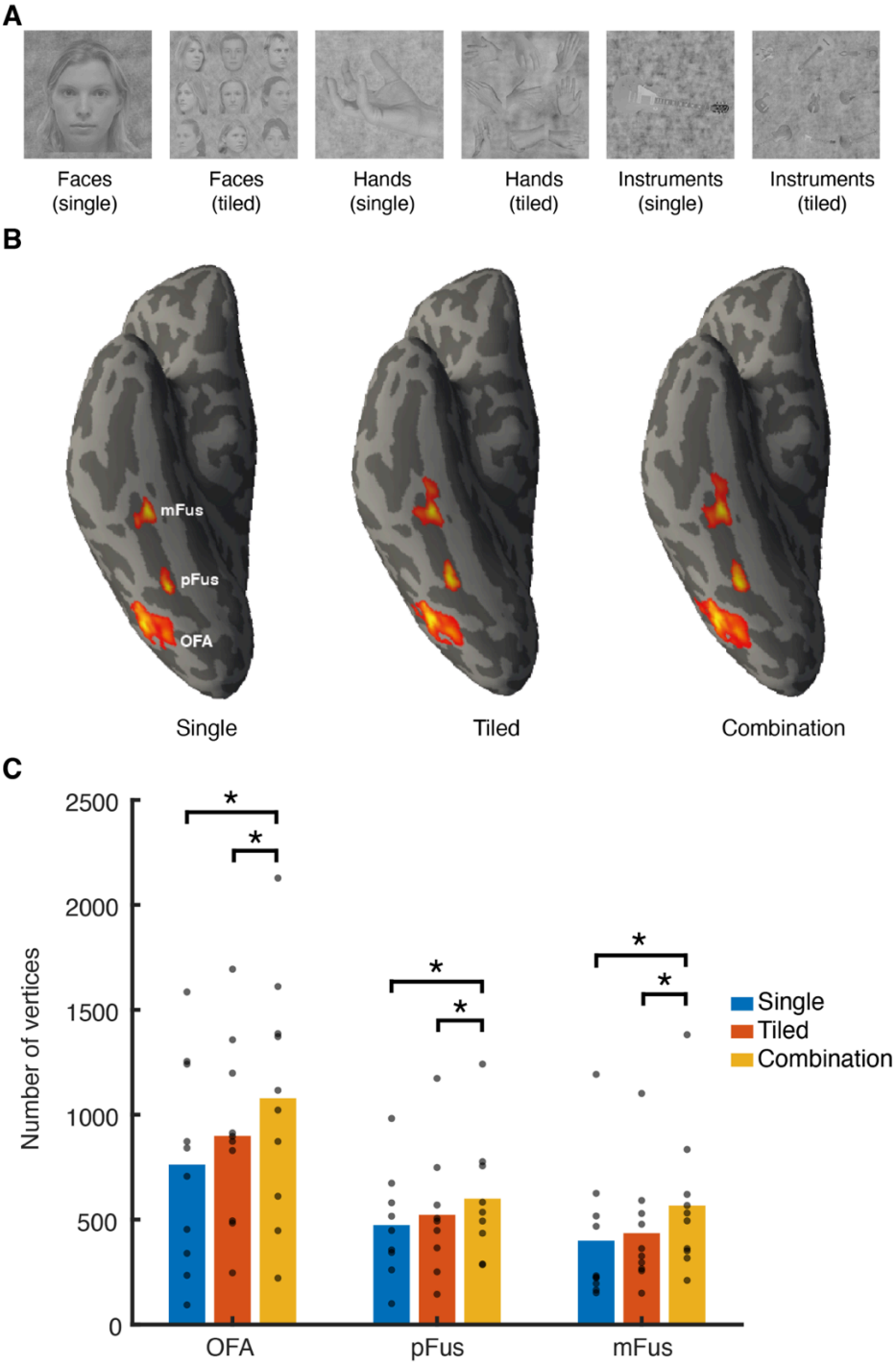

Figure S1. The localisation of face-selective brain regions. **A.** Stimuli used for the six image categories in the localiser runs. **B.** Face-selective regions OFA, pFus and mFus on the ventral surface of the right hemisphere in an example participant, defined using different localisation stimuli (single faces vs. single hands and instruments, tiled comparisons, or the combination of both single and tiled). In each case, ROIs have the same central location, with the activation spread out over a different amount of the cortical surface depending on the localisation approach. **C.** The number of vertices in each face-selective ROI, delineated using localiser stimuli consisting of single faces, tiled faces, or the combination of both. Dots show individuals and bars the mean number of vertices. Asterisks show significant differences ($p < .05$).

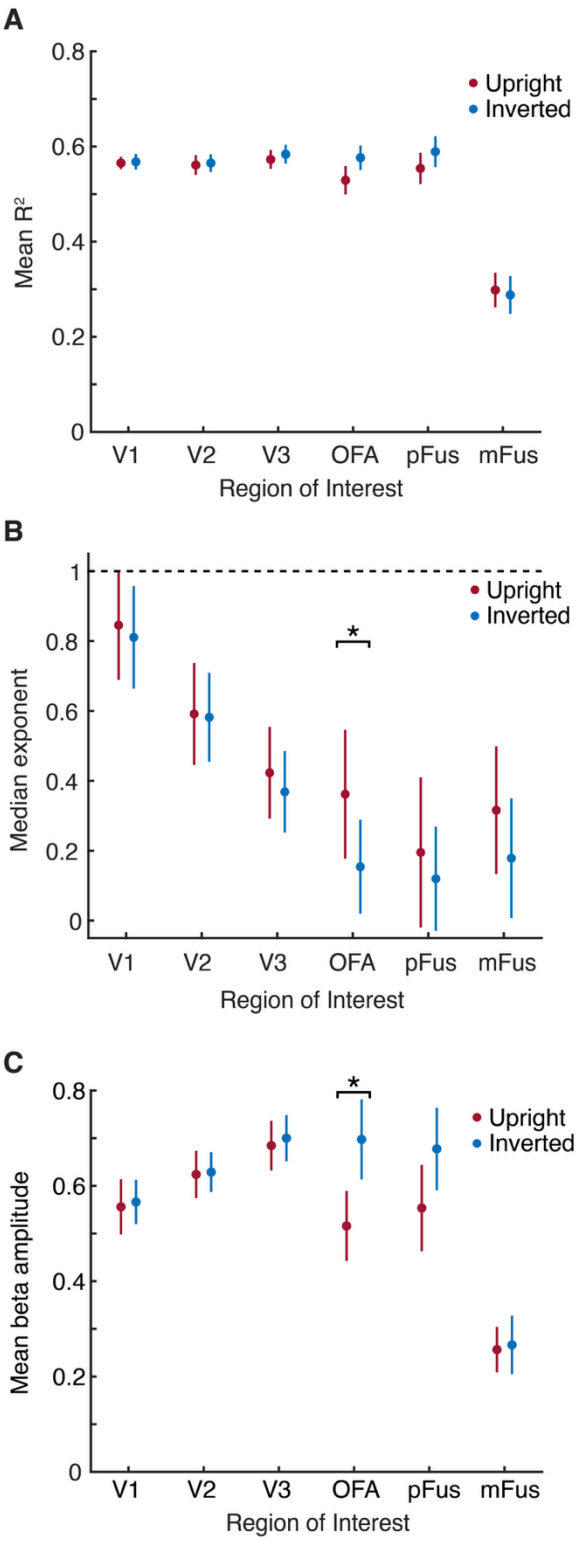

Figure S2. A. Mean R^2 values for the compressive spatial summation (CSS) pRF model for upright (red) and inverted (blue) faces in each of the ROIs. Error bars show the SEM. **B.** Median exponent values for the CSS model in each ROI, plotted as in panel A. The dashed line represents linear summation, with all values < 1 indicating compression. Exponent values are lower (indicating increased compression) in face-selective regions compared to V1-V3, as in Kay et al. (2013). The asterisk denotes a statistically significant difference ($p < .05$). **C.** Mean beta amplitudes for the CSS model in each ROI, plotted as in other panels.

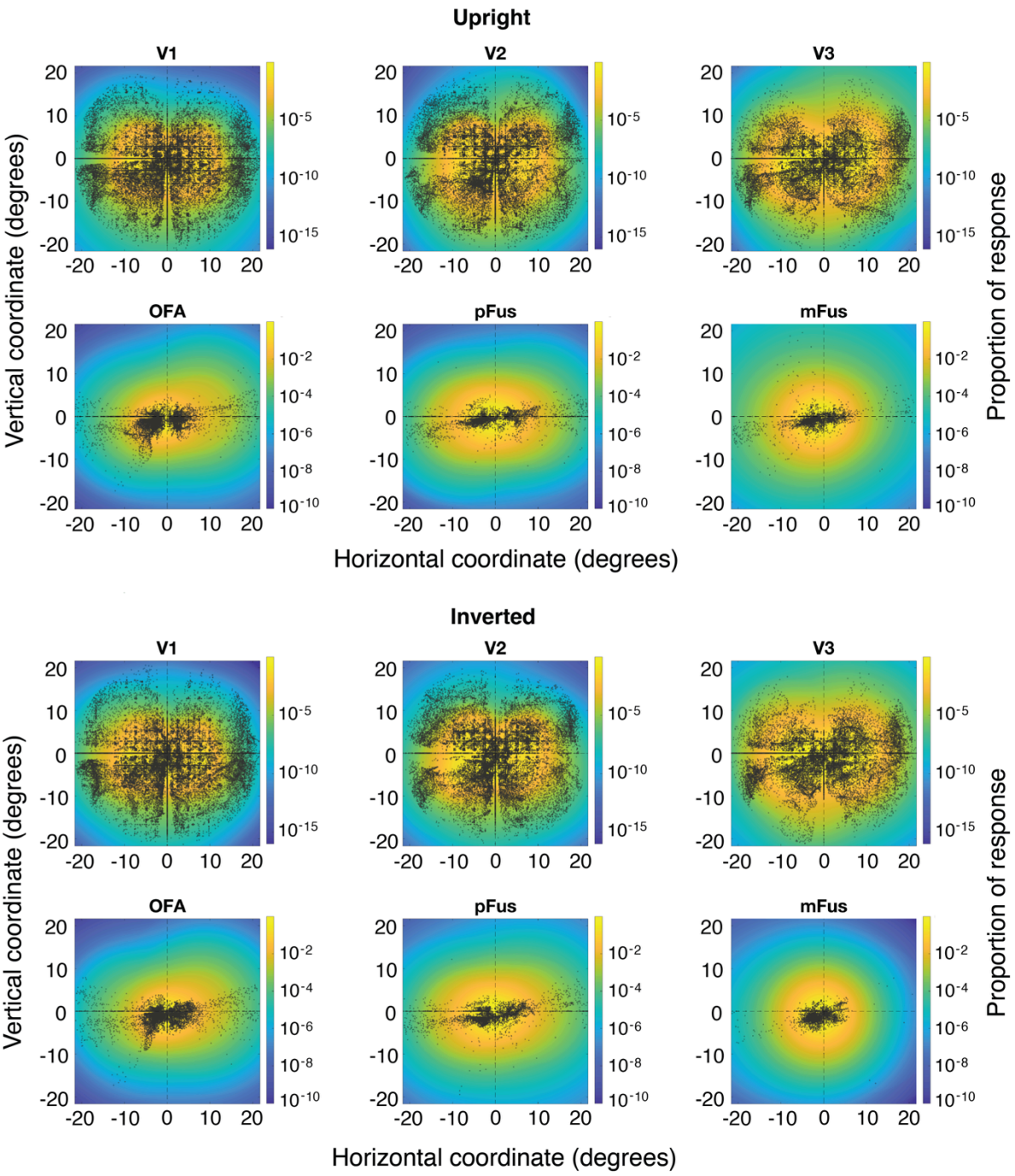

Figure S3. Mean visual field coverage for upright (top) and inverted (bottom) faces. Coordinates represent eccentricity in degrees of visual angle, with negative values for the left/lower and positive values for the right/upper visual field. Values were converted to log scale before plotting, for visualisation purposes (see colour bar). Dots represent pRF centres from all participants. For plots without pRF centres imposed, see Figure S3. These plots show the relative responsiveness of pRFs across the visual field, incorporating the number, size, and spatial profile of each pRF within the population of vertices that responded to each stimulus.

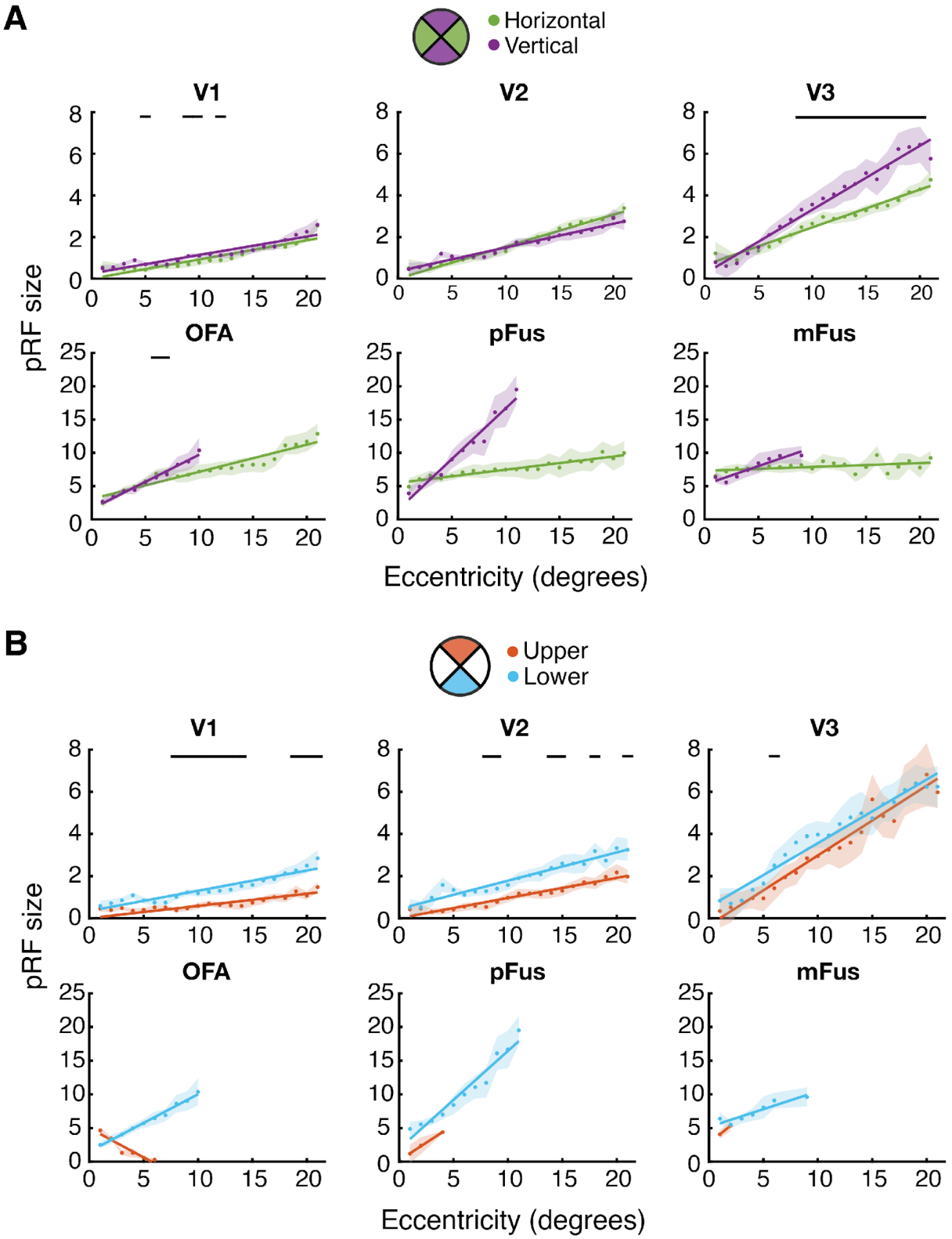

Figure S4. Mean pRF size across eccentricity measured with inverted faces, plotted along the horizontal (green) and vertical (purple) meridians **(A)** and in the upper and lower visual field **(B)**. At each eccentricity, size estimates were only plotted if they were averaged from at least five vertices. Black lines indicate significant differences according to location ($p < .05$).

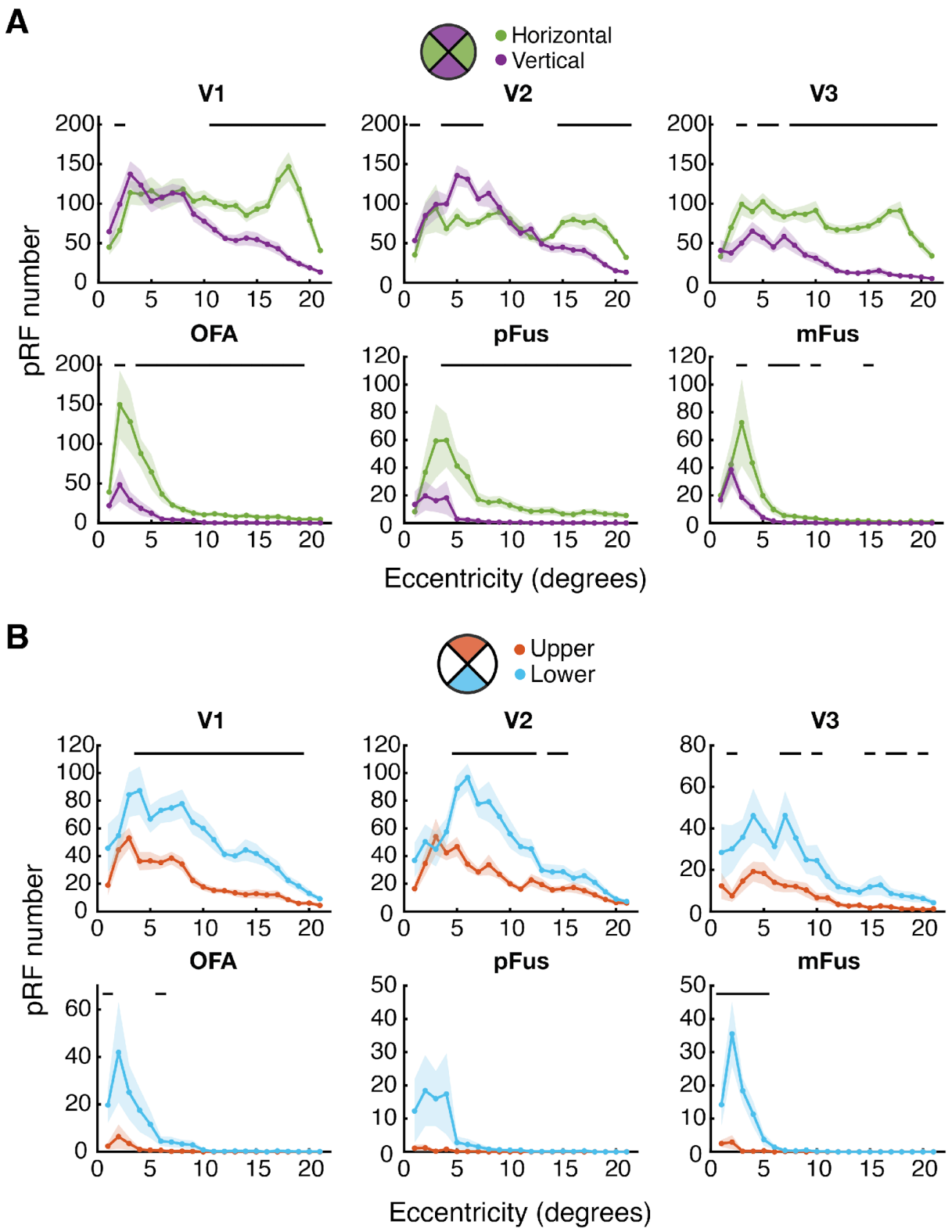

Figure S5. Mean pRF number for inverted faces, plotted across eccentricity on the horizontal (green) and vertical (purple) meridians **(A)** and in the upper and lower visual field **(B)**. Black lines indicate significant differences according to location ($p < .05$).

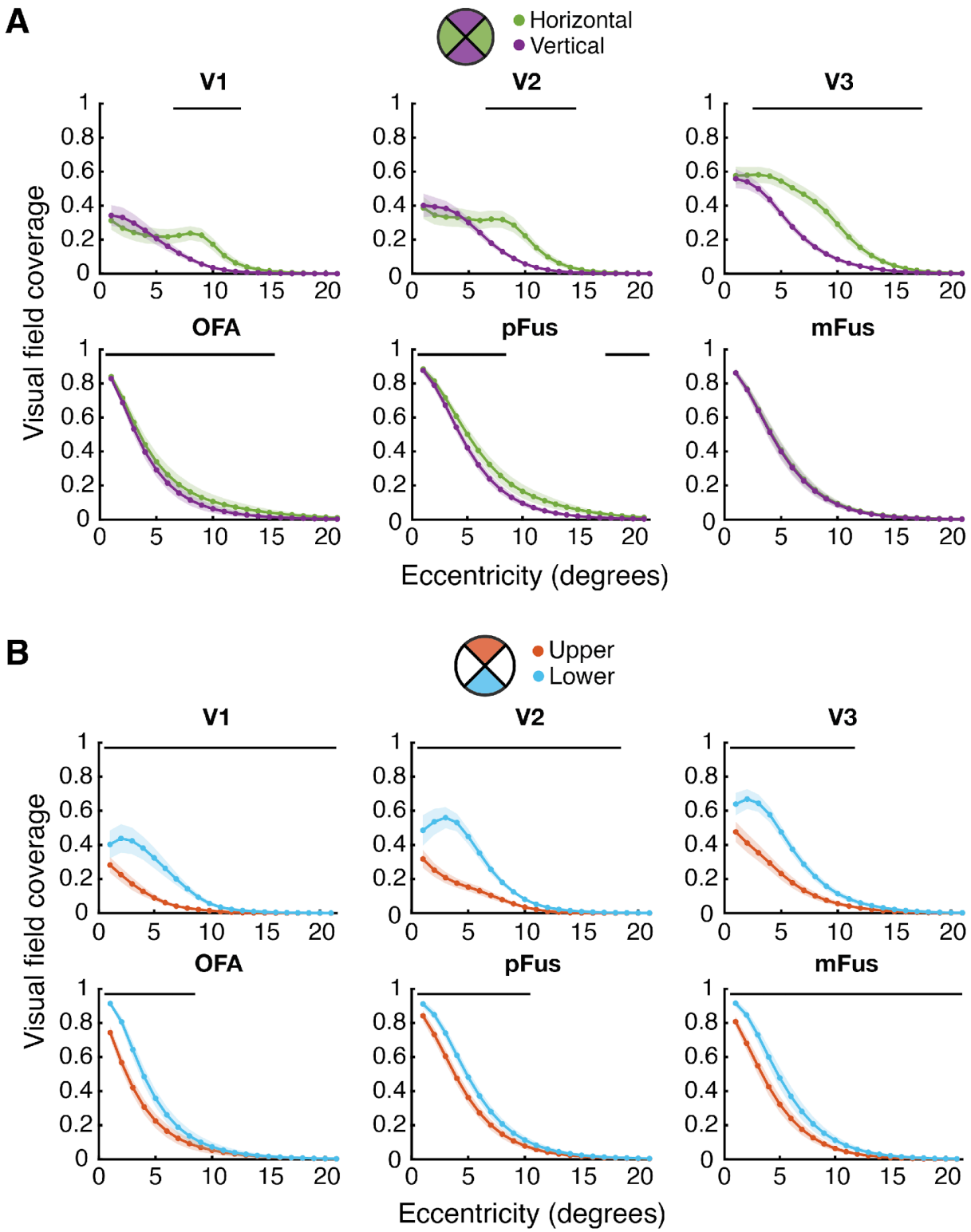

Figure S6. Visual field coverage for inverted faces, plotted across eccentricity on the horizontal (green) and vertical (purple) meridians **(A)** and in the upper and lower visual field **(B)**. At each eccentricity, size estimates were only plotted if they were averaged from at least five vertices. Black lines indicate significant differences according to location ($p < .05$).

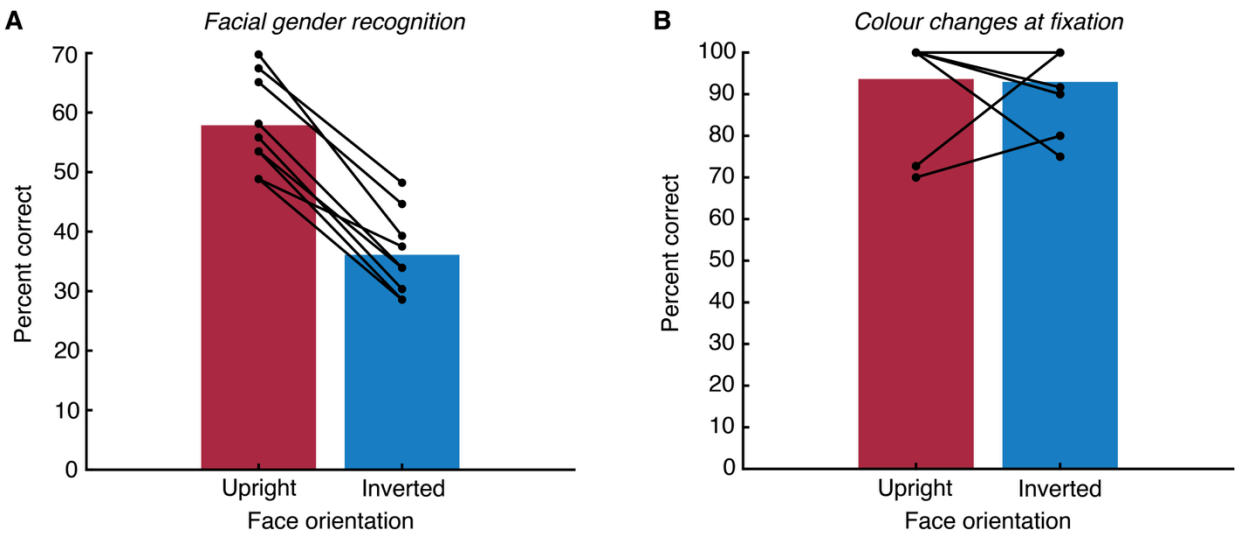

Figure S7. Behavioural results as a function of face orientation within the bar stimuli used to measure pRFs. **A.** Percent-correct recognition performance on the facial gender recognition task, showing the percentage of correctly identified male bars. Dots show individual data, with lines joining each participant's performance for upright and inverted faces. A clear inversion effect is seen, with worst performance for inverted faces. **B.** Percent-correct recognition performance on the fixation task during the pRF experiment, showing the percentage of fixation cross colour changes that were correctly detected. Dots show individual data, with lines joining each participant's performance for the fixation task during the presentation of upright and inverted faces. Four participants had 100% correct in both the upright and inverted runs. On the whole, there is no difference in performance when faces were upright vs. inverted.

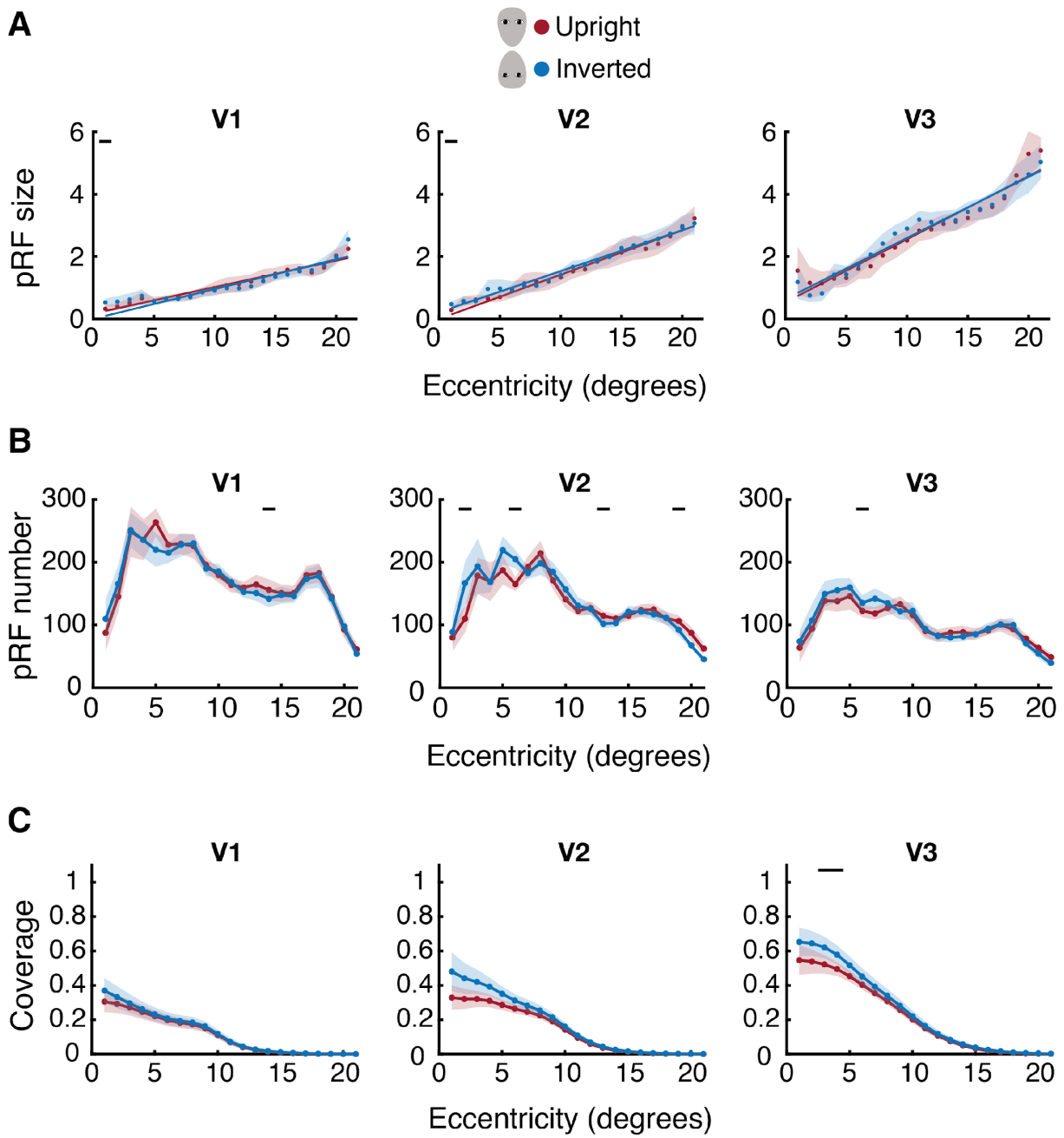

Figure S8. The effect of face orientation on spatial selectivity in early visual cortex. **A.** Mean pRF sizes in V1-V3, plotted across eccentricity for upright (red) and inverted (blue) faces. Black lines indicate significant differences in each property according to face inversion ($p < .05$). There were no significant main effects of inversion in any area (V1: β = -0.01 [-0.20, 0.18], p = .910; V2: β = 0.08 [-0.19, 0.34], p = .570; V3: β = 0.03 [-0.33, 0.40], p = .856). **B.** pRF number, plotted as in panel A. Main effects of inversion were again non-significant in all areas (V1: $F_{1,180}$ = 0.32, p = .583; V2: $F_{1,180}$ = 2.17, p = .175; V3: $F_{1,180}$ = 1.45, p = .259). **C.** Visual field coverage, plotted as in panel A. Main effects of inversion were again non-significant in all areas (all F<1).

References

Abrams J, Nizam A, Carrasco M (2012) Isoeccentric locations are not equivalent: the extent of the vertical meridian asymmetry. Vision Res 52:70-78.

Alvarez I, de Haas B, Clark CA, Rees G, Schwarzkopf DS (2015) Comparing different stimulus configurations for population receptive field mapping in human fMRI. Front Hum Neurosci 9:96.

Amano K, Wandell BA, Dumoulin SO (2009) Visual field maps, population receptive field sizes, and visual field coverage in the human MT+ complex. J Neurophysiol 102:2704-2718.

Anderson EJ, Tibber MS, Schwarzkopf DS, Shergill SS, Fernandez-Egea E, Rees G, Dakin SC (2017) Visual population receptive fields in people with schizophrenia have reduced inhibitory surrounds. J Neurosci 37:1546-1556.

Avidan G, Behrmann M (2021) Spatial integration in normal face processing and its breakdown in congenital prosopagnosia. Annual Review of Vision Science 7:301-321.

Barbot A, Xue S, Carrasco M (2021) Asymmetries in visual acuity around the visual field. Journal of Vision 21:2.

Benson NC, Kupers ER, Barbot A, Carrasco M, Winawer J (2021) Cortical magnification in human visual cortex parallels task performance around the visual field. eLife 10.

Boucart M, Lenoble Q, Quettelart J, Szaffarczyk S, Despretz P, Thorpe SJ (2016) Finding faces, animals, and vehicles in far peripheral vision. Journal of Vision 16:1-13.

Brainard DH (1997) The psychophysics toolbox. Spat Vis 10:433-436.

Bruce V, Young A (1986) Understanding face recognition. Br J Psychol 77(3):305-327.

Carrasco M, Talgar CP, Cameron EL (2001) Characterizing visual performance fields: effects of transient covert attention, spatial frequency, eccentricity, task and set size. Spat Vis 15:61-75.

Cox RW (1996) AFNI: software for analysis and visualization of functional magnetic resonance neuroimages. Comput Biomed Res 29:162-173.

Crouzet SM, Kirchner H, Thorpe SJ (2010) Fast saccades toward faces: face detection in just 100 ms. Journal of Vision 10:1-17.

Dale AM, Fischl B, Sereno MI (1999) Cortical surface-based analysis. I. Segmentation and surface reconstruction. NeuroImage 9:179-194.

de Haas B, Schwarzkopf DS, Alvarez I, Lawson RP, Henriksson L, Kriegeskorte N, Rees G (2016) Perception and Processing of Faces in the Human Brain Is Tuned to Typical Feature Locations. The Journal of Neuroscience 36:9289-9302.

DeYoe EA, Bandettini P, Neitz J, Miller D, Winans P (1994) Functional magnetic resonance imaging (FMRI) of the human brain. J Neurosci Methods 54:171-187.

Dumoulin SO, Wandell BA (2008) Population receptive field estimates in human visual cortex. NeuroImage 39:647-660.

Duncan RO, Boynton GM (2003) Cortical magnification within human primary visual cortex correlates with acuity thresholds. Neuron 38:659-671.

Engel SA, Glover GH, Wandell BA (1997) Retinotopic organisation in human visual cortex and the spatial precision of functional MRI. Cereb Cortex 7:181-192.

Fang F, Murray SO, He S (2007) Duration-dependent fMRI adaptation and distributed viewer-centered face representation in human visual cortex. Cerebral Cortex 17:1402-1411.

Finzi D, Gomez J, Nordt M, Rezai AA, Poltoratski S, Grill-Spector K (2021) Differential spatial computations in ventral and lateral face-selective regions are scaffolded by structural connections. Nature Communications 12:2278.

Fischl B (2012) FreeSurfer. NeuroImage 62:774-781.

Fischl B, Sereno MI, Dale AM (1999) Cortical surface-based analysis. II: Inflation, flattening, and a surface-based coordinate system. NeuroImage 9:195-207.

Greenwood JA, Szinte M, Sayim B, Cavanagh P (2017) Variations in crowding, saccadic precision, and spatial localization reveal the shared topology of spatial vision. Proceedings of the National Academy of Sciences 114:E3573-E3582.

Grill-Spector K, Weiner KS, Kay K, Gomez J (2017) The Functional Neuroanatomy of Human Face Perception. Annual Review of Vision Science 3:167-196.

Groen IIA, Dekker TM, Knapen T, Silson EH (2022) Visuospatial coding as ubiquitous scaffolding for human cognition. Trends Cogn Sci 26:81-96.

Haxby JV, Hoffman EA, Gobbini MI (2000) The distributed human neural system for face perception. Trends Cogn Sci 4:223-233.

Henson RN (2016) Repetition suppression to faces in the fusiform face area: A personal and dynamic journey. Cortex 80:174-184.

Himmelberg MM, Winawer J, Carrasco M (2020) Stimulus-dependent contrast sensitivity asymmetries around the visual field. Journal of Vision 20:18.

Himmelberg MM, Winawer J, Carrasco M (2023a) Polar angle asymmetries in visual perception and neural architecture. Trends Neurosci 46:445-458.

Himmelberg MM, Tuncok E, Gomez J, Grill-Spector K, Carrasco M, Winawer J (2023b) Comparing retinotopic maps of children and adults reveals a late-stage change in how V1 samples the visual field. Nature Communications 14:1561.

Hughes AE, Greenwood JA, Finlayson NJ, Schwarzkopf DS (2019) Population receptive field estimates for motion-defined stimuli. NeuroImage 199:245-260.

Kalpadakis-Smith AV, Goffaux V, Greenwood JA (2018) Crowding for faces is determined by visual (not holistic) similarity: Evidence from judgements of eye position. Sci Rep 8:12556.

Kanwisher N, McDermott J, Chun MM (1997) The fusiform face area: a module in human extrastriate cortex specialized for face perception. The Journal of Neuroscience 17:4302-4311.

Kanwisher N, Tong F, Nakayama K (1998) The effect of face inversion on the human fusiform face area. Cognition 68:B1-B11.

Kay KN, Weiner KS, Grill-Spector K (2015) Attention reduces spatial uncertainty in human ventral temporal cortex. Curr Biol 25:595-600.

Kay KN, Winawer J, Mezer A, Wandell BA (2013) Compressive spatial summation in human visual cortex. J Neurophysiol 110:481-494.

Kleiner M, Brainard D, Pelli D (2007) What's new in Psychtoolbox-3?

Kovacs P, Knakker B, Hermann P, Kovacs G, Vidnyanszky Z (2017) Face inversion reveals holistic processing of peripheral faces. Cortex 97:81-95.

Kurzawski JW, Burchell A, Thapa D, Majaj NJ, Winawer JA, Pelli DG (2021) An enhanced Bouma model fits a hundred people's visual crowding. bioRxiv.

Langner O, Dotsch R, Bijlstra G, Wigboldus DHJ, Hawk ST, van Knippenberg A (2010) Presentation and validation of the Radboud Faces Database. Cogn Emot 24:1377-1388.

Le Grand R, Mondloch CJ, Maurer D, Brent HP (2001) Early visual experience and face processing. Nature 410:890.

Linhardt D, Pawloff M, Hummer A, Woletz M, Tik M, Ritter M, Schmidt-Erfurth U, Windischberger C (2021) Combining stimulus types for improved coverage in population receptive field mapping. NeuroImage 238:118240.

Louie EG, Bressler DW, Whitney D (2007) Holistic crowding: Selective interference between configural representations of faces in crowded scenes. Journal of Vision 7(2):24:1-11.

Mäkelä P, Näsänen R, Rovamo J, Melmoth D (2001) Identification of facial images in peripheral vision. Vision Res 41:599-610.

McKone E (2004) Isolating the special component of face recognition: peripheral identification and a Mooney face. Journal of Experimental Psychology: Learning, Memory, and Cognition 30:181-197.

McKone E (2009) Holistic processing for faces operates over a wide range of sizes but is strongest at identification rather than conversational distances. Vision Res 49:268-283.

Miller KD (2016) Canonical computations of cerebral cortex. Curr Opin Neurobiol 37:75-84.

Morsi AY, Goffaux V, Greenwood JA (2024) The resolution of face perception varies systematically across the visual field. PLoS One 19:e0303400.

Natu VS, Barnett MA, Hartley J, Gomez J, Stigliani A, Grill-Spector K (2016) Development of Neural Sensitivity to Face Identity Correlates with Perceptual Discriminability. The Journal of Neuroscience 36:10893-10907.

Nelder JA, Mead R (1965) A Simplex-Method for Function Minimization. Computer Journal 7:308-313.

Pelli DG (1997) The VideoToolbox software for visual psychophysics: Transforming numbers into movies. Spat Vis 10:437-442.

Penny WD, Friston KJ, Ashburner JT, Kiebel SJ, Nichols TE (2011) Statistical parametric mapping: The analysis of functional brain images. Amsterdam: Academic Press.

Petras K, Ten Oever S, Jacobs C, Goffaux V (2019) Coarse-to-fine information integration in human vision. NeuroImage 186:103-112.

Poltoratski S, Kay K, Finzi D, Grill-Spector K (2021) Holistic face recognition is an emergent phenomenon of spatial processing in face-selective regions. Nature Communications 12:4745.

Rossion B (2008) Picture-plane inversion leads to qualitative changes of face perception. Acta Psychol (Amst) 128:274-289.

Rossion B, Gauthier I (2002) How does the brain process upright and inverted faces? Behav Cogn Neurosci Rev 1:63-75.

Roux-Sibilon A, Peyrin C, Greenwood JA, Goffaux V (2023) Radial bias in face identification. Proceedings of the Royal Society B: Biological Sciences 290:20231118.

Schuurmans JP, Bennett MA, Petras K, Goffaux V (2023) Backward masking reveals coarse-to-fine dynamics in human V1. NeuroImage 274:120139.

Schwarzkopf DS (2022) SamSrf 9.4 - Matlab toolbox for pRF analysis.

Schwarzkopf DS, Anderson EJ, de Haas B, White SJ, Rees G (2014) Larger extrastriate population receptive fields in autism spectrum disorders. The Journal of Neuroscience 34:2713-2724.

Sereno MI, Dale AM, Reppas JB, Kwong KK, Belliveau JW, Brady TJ, Rosen BR, Tootell RB (1995) Borders of multiple visual areas in humans revealed by functional magnetic resonance imaging. Science 268:889-893.

Silson EH, Groen IIA, Baker CI (2022) Direct comparison of contralateral bias and face/scene selectivity in human occipitotemporal cortex. Brain Structure and Function 227:1405-1421.

Silson EH, Reynolds RC, Kravitz DJ, Baker CI (2018) Differential sampling of visual space in ventral and dorsal early visual cortex. The Journal of Neuroscience 38:2294-2303.

Silson EH, Chan AW-Y, Reynolds RC, Kravitz DJ, Baker CI (2015) A retinotopic basis for the division of high-level scene processing between lateral and ventral human occipitotemporal cortex. J Neurosci 35:11921-11935.

Silva MF, Brascamp JW, Ferreira S, Castelo-Branco M, Dumoulin SO, Harvey BM (2018) Radial asymmetries in population receptive field size and cortical magnification factor in early visual cortex. NeuroImage 167:41-52.

Silva MF, Harvey BM, Jorge L, Canário N, Machado F, Soares M, d'Almeida OC, Castelo-Branco M (2021) Simultaneous changes in visual acuity, cortical population receptive field size, visual field map size, and retinal thickness in healthy human aging. Brain Structure and Function 226:2839-2853.

Stigliani A, Weiner KS, Grill-Spector K (2015) Temporal Processing Capacity in High-Level Visual Cortex Is Domain Specific. The Journal of Neuroscience 35:12412–12424.

Tanaka K (1996) Inferotemporal cortex and object vision. Annu Rev Neurosci 19:109-139.

van Dijk JA, de Haas B, Moutsiana C, Schwarzkopf DS (2016) Intersession reliability of population receptive field estimates. NeuroImage 143:293-303.

Weiner KS, Grill-Spector K (2010) Sparsely-distributed organization of face and limb activations in human ventral temporal cortex. NeuroImage 52:1559-1573.

Westheimer G (2003) The distribution of preferred orientations in the peripheral visual field. Vision Res 43:53-57.

Witthoft N, Poltoratski S, Nguyen M, Golarai G, Liberman A, LaRocque KF, Smith ME, Grill-Spector K (2016) Reduced spatial integration in the ventral visual cortex underlies face recognition deficits in developmental prosopagnosia. BioRxiv 051102.

Yin RK (1969) Looking at upside-down faces. J Exp Psychol 81:141.